
# CATHODOLUMINESCENCE OF IRRADIATED HAFNIUM DIOXIDE

THESIS

Emily A. Purcell, Second Lieutenant, USAF

AFIT/GAP/ENP/11-M08

**DEPARTMENT OF THE AIR FORCE**
**AIR UNIVERSITY**

## AIR FORCE INSTITUTE OF TECHNOLOGY

**Wright-Patterson Air Force Base, Ohio**

AFIT/GAP/ENP/11-M08

# CATHODOLUMINESCENCE OF IRRADIATED HAFNIUM DIOXIDE

THESIS

Presented to the Faculty

Department of Engineering Physics

Graduate School of Engineering and Management

Air Force Institute of Technology

Air University

Air Education and Training Command

In Partial Fulfillment of the Requirements for the

Degree of Master of Science in Applied Physics

Emily A. Purcell, BS

Second Lieutenant, USAF

March 2011

AFIT/GAP/ENP/11-M08

# CATHODOLUMINESCENCE OF IRRADIATED HAFNIUM DIOXIDE

Emily A. Purcell, BS
Second Lieutenant, USAF

Approved:

| | |
|---|---|
| Robert L. Hengehold, PhD (Chairman) | 7 Mar 2011<br>Date |
| Nancy C. Giles, PhD (Member) | 7 Mar 2011<br>Date |
| LTC John W. McClory (Member) | 7 MAR 2011<br>Date |

## Abstract

Hafnium dioxide ($HfO_2$) is increasingly being used in place of silicon dioxide as a gate insulator in field effect transistors. This is primarily due to its high dielectric constant, κ, of 25 (silicon oxide has a dielectric constant of 3.9). This higher κ results in a higher capacitance in the gate without decreasing its thickness, which can lead to current leakage in the device. Additionally, a higher κ allows one to maintain the same capacitance while decreasing the surface area, allowing the devices to be built much smaller than previously possible. Since these devices may be employed in radiation environments, it is important to understand the effects that radiation may have on the reliability of such devices. The goal of this research is to determine the effects of gamma, neutron, and ion radiation on $HfO_2$.

Cathodoluminescence (CL) was used to study the $HfO_2$ samples, both before and after irradiation. The CL system was equipped with a Kimball Physics EMG-12 electron gun with beam energies ranging from 1 keV to 20 keV and beam currents ranging from 10 μA to 50 μA. A Monte Carlo calculation using CASINO software was performed in order to determine the beam energy for the desired depth of penetration. Measurements were taken at sample temperatures ranging from 7K (closed cycled cryostat) to 300K (room temperature), as well as at various beam energies and beam currents.

The samples examined were grown by either atomic layer deposition (ALD) or pulsed laser deposition (PLD); the PLD samples were deposited on substrates maintained at varying temperatures during deposition (300°C, 500°C, and 750°C), the AQLD samples on substrates at 250°C. It was found that the ALD samples had a much more

consistent thickness than the PLD samples, as evidenced by Rutherford backscattering spectroscopy (RBS) profiles and color variations in PLD samples that were not present in ALD samples. In addition, CL confirmed earlier x-ray diffraction (XRD) data indicating that the PLD samples grown at 750°C and 500°C were superior to those grown at 300°C.

A wide range of measurements have been made; however, agreement with published data is generally lacking at this point. In addition, to date, spectra from irradiated samples show little change from the unirradiated samples, possibly due to the fact that the ion doses used were insufficient to cause observable damage. As a result, experimental results are inconclusive as to the effects radiation had on either the ALD or PLD samples. On the other hand, definite information was obtained as to the quality of the PLD samples grown at different substrate temperatures as well as to the quality of the ALD samples vis-à-vis the PLD samples.

**Acknowledgments**

First and foremost, I would like to thank my thesis advisor, Dr. Robert Hengehold, for his patience, kindness, and dedication, in addition to all the knowledge he has shared with me. I would also like to thank the lab technicians, Greg Smith and Mike Ranft, for the countless hours they put in making sure my experiment was working properly, and also in helping me to understand how everything works. Many thanks go to Captain Jesse Foster for providing me with the irradiated samples, and for all the time he has spent helping me understand the irradiation methods. Finally, I would like to thank Jacob Martin and Michael Rhoby for their hard work in fixing assorted problems that cropped up during the course of my thesis work.

Emily A. Purcell

## Table of Contents

Page

Page

## List of Figures

Figure Page

Figure Page

Figure Page

## List of Tables

Table Page

CATHODOLUMINESCENCE OF IRRADIATED HAFNIUM DIOXIDE

# I. Introduction

## General Issue

It is well-known that radiation can have detrimental effects on semiconductor devices, causing such devices to fail. Since such devices are often used in satellites, which must operate in a high radiation environment (i.e. space), it is desirable to understand the effects of radiation on materials that are used in these devices. Specifically, hafnium dioxide ($HfO_2$) is a promising insulator material for such devices because of its high dielectric constant of 25, which allows for a smaller surface area (with a given capacitance and thickness) than its silicon oxide ($SiO_2$) predecessor (dielectric constant of 3.9). However, if $HfO_2$ is to be useful, the effects of radiation damage must be better understood. For this reason, this thesis will investigate the effects of gamma rays, neutrons, and ions on $HfO_2$ using cathodoluminescence (CL) as the means of investigation. Additionally, there are several different ways of growing $HfO_2$, and the resulting material may or may not be affected by radiation in different ways. In this thesis, we will also investigate $HfO_2$ films produced by two common growth methods,

atomic layer deposition (ALD) and pulsed laser deposition (PLD), particularly the effects of different growth conditions on the spectra of these samples.

**Problem Statement**

The goals of this thesis are: (1) to examine the radiation hardness of hafnium dioxide against gamma, neutron, and ion irradiation, (2) to compare the properties of $HfO_2$ grown at assorted substrate temperatures for PLD, and (3) to compare the properties of $HfO_2$ grown by PLD with those grown by atomic layer deposition (ALD).

**Research Focus**

This research will be focused on PLD samples of $HfO_2$ that were grown at substrate temperatures of 300°C, 500°C, and 750°C, as well as ALD samples of $HfO_2$ that were deposited at a substrate temperature of 250°C. The PLD samples will also be examined after exposure to the three types of radiation previously mentioned, and the ALD samples will be examined after exposure to nitrogen and silicon ion irradiation. Both growth methods utilize silicon (Si) as the substrate material. The thickness of the ALD samples is known to be precisely 50 nm from Rutherford backscattering spectrometry (RBS). The thickness of the PLD samples averaged approximately 100 nm. As far as radiation damage is concerned, we do not expect to see any residual damage as a result of gamma irradiation, but there is a possibility of seeing residual damage from the neutron and ion irradiation, either in the form of decreased intensity in the spectra, or in the creation of new features in the spectra.

**Methodology**

Cathodoluminescence was the experimental technique chosen to determine the optical properties of the material. This technique involves exciting luminescence from the sample using electron beam excitation from a low (500 eV to 20 keV) energy electron gun. This gun, along with a copper sample holder attached to a liquid He refrigerator, and the samples, were mounted in a high vacuum chamber capable of pressures as low as $1 \times 10^{-7}$ torr. The luminescence resulting from the electron excitation was analyzed using a grating spectrometer, a photomultiplier tube, and SynerJY data acquisition software.

**Motivation**

The United States Air Force has many space-based interests, from its space vehicles to global positioning system (GPS) satellites to communication satellites. These systems use semiconductor devices, which can be negatively affected by the radiation environment present in orbit.

Current efforts also seek to maintain capacitance while decreasing size in terms of surface area. Capacitance of a semiconductor device is very nearly described by that of an infinite parallel plate capacitor, with

$$C = \frac{\varepsilon_0 \kappa A}{d} \tag{1.1}$$

where $C$ is capacitance in Farads, $\varepsilon_0$ is the permittivity of free space, 8.85E-12 Farads per meter, $\kappa$ is the dielectric constant and is dimensionless, $A$ is the area of the of the material in square meters, and $d$ is the thickness of the material in meters. It is apparent that a decrease in $d$ allows for a smaller $A$ for a given $C$, but the insulator can only become so thin before tunneling occurs, which causes high power consumption and

reduced device reliability. The only other variable in this equation is κ; if one chooses a material with a larger κ, then one can decrease the surface area without decreasing the thickness or capacitance. As previously mentioned, $SiO_2$ has a dielectric constant of 3.9. $HfO_2$, with its dielectric constant of more than six times that of $SiO_2$, would therefore allow for a decrease in area of that same factor when replacing $SiO_2$ with $HfO_2$.

# II. Background

## Chapter Overview

The purpose of this chapter is to discuss relevant research that has already been conducted on $HfO_2$ as well as the theory pertaining to cathodoluminescence. The two types of growth methods being examined will also be addressed. Finally, the theory of the types of irradiation performed on the $HfO_2$ samples will be discussed, along with the damage they are expected to cause in materials.

## Solid State Physics Overview

Solid-state physics is the study of rigid matter; it studies how the macroscopic properties of materials result from their microscopic (atomic-scale) properties. Crystal structure, interatomic forces, lattice vibrations, and dispersion relations are a few of the properties examined in solid-state physics.

The crystal structure of $HfO_2$ can be found in four different forms: monoclinic, tetragonal, and cubic [1], as well as orthorhombic [2]. The structure is found to be dependent on the temperature during growth; monoclinic occurs at low temperatures, cubic at higher temperatures, and tetragonal at intermediate temperatures [1]. Substrate temperature was not mentioned for the orthorhombic structure; however, it is suggested that it should be possible to stabilize the orthorhombic structure at ambient pressure, where the orthorhombic phase results from the nanometer size of the particles [2].

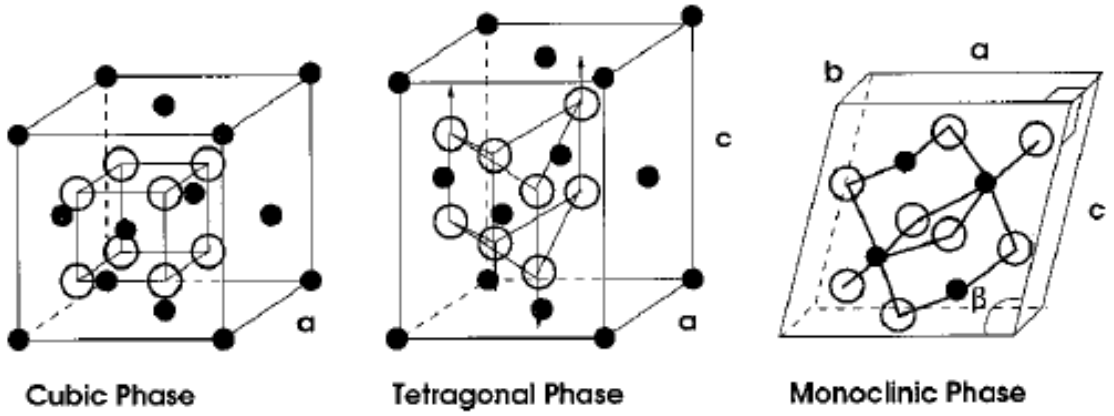


**Figure 1. Diagram of three possible crystal structures of $HfO_2$ [1]. The orthorhombic phase, not pictured here, has also been cited as a possible phase for $HfO_2$ [2].**

Materials can be put into one of three different categories: conductors, semiconductors, and insulators. Conductors readily allow current to flow because of their overlapping valence and conduction bands. Insulators resist the flow of current because it takes a large amount of energy to excite an electron from the valence band to the conduction band. A semiconductor falls in between a conductor and an insulator, where it is easier to excite the flow of electrons than in an insulator, but not quite as easy as in a conductor. $HfO_2$, having a large band gap, is an insulator (also known as a dielectric material, discussed above).

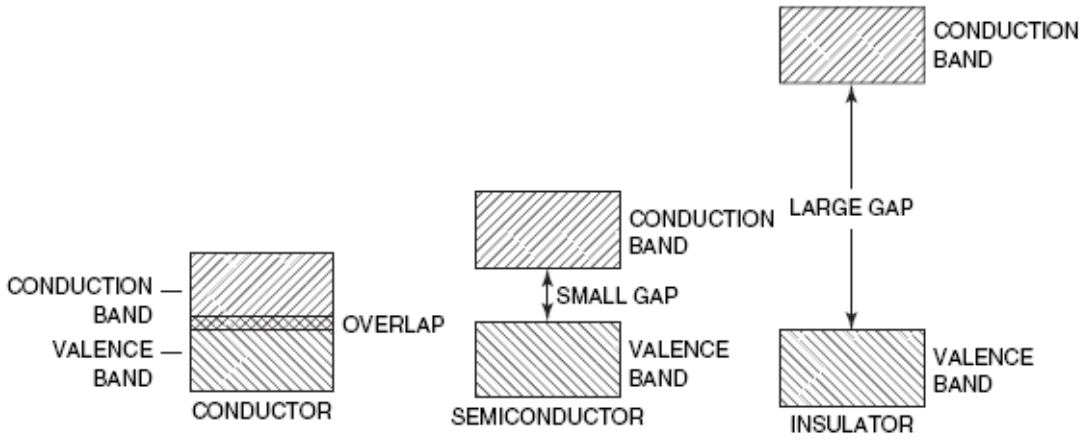


**Figure 2. Energy band diagram for conductors, semiconductors, and insulators. The "gap" refers to the band gap energy of the materials [3].**

When an electron is excited, it moves from the valence band to the conduction band, creating a hole in the valence band and an extra electron in the conduction band; this is known as an electron-hole (e-h) pair. When the electron and the hole recombine, energy is released, which will be discussed in more detail later.

### X-Ray Diffraction

The following discussion of x-ray diffraction (XRD) is taken from B. D. Cullity's *Elements of X-Ray Diffraction* [4]. One tool used to investigate the fine structure of matter is x-ray diffraction, which utilizes the fact that crystals diffract x-rays, as discovered by Max von Laue in 1912. The manner in which the x-rays are diffracted reveals the structure of the crystal. The x-ray region of the electromagnetic spectrum lies approximately in the range 0.5-2.5Å. X-rays are produced when any electrically charged particle of sufficient kinetic energy is rapidly decelerated.

"A crystal may be defined as a solid composed of atoms arranged in a pattern periodic in three dimensions" [4]. A solid may also be amorphous, with no predictable

arrangement of atoms. One may consider a crystal's lattice instead of the actual atoms composing the crystal; the lattice is the framework on which the crystal is built. Excluding amorphous, there are fourteen allowable crystal structures: simple, body-centered, or face-centered cubic, simple or body-centered tetragonal, simple, body-centered, base-centered, or face-centered orthorhombic, trigonal, hexagonal, simple or base-centered monoclinic, and triclinic. These are known as Bravais lattices.

Diffraction is the result of electromagnetic waves starting out in phase and rejoining with some phase difference, usually the result of the waves having different optical path lengths before rejoining. If the path length is different by an integer wavelength, though, the waves will still be in phase. The atoms that comprise the crystal will scatter the incident x-rays in all directions, with some directions producing beams that are in phase. The condition that produces rays that are completely in phase is

$$n\lambda = 2d\sin(\theta), \tag{2.1}$$

with θ being the angle of incidence and $d$ being distance between planes in the crystal; $n$ is the order of reflection which may be any integral value that does not force sin(θ) to be greater than unity. This relationship is known as the Bragg law; this condition must be met if diffraction is to occur. Waves that are out of phase will cause destructive interference, thus annulling one another. Diffraction, therefore, can only occur at certain angles of incidence. If one holds the wavelength fixed and scans over θ, the lattice spacing can be determined for a given axis of rotation of the crystal; this is known as the rotating-crystal method. One can then determine the structure of the crystal based on the angles that cause diffraction.

**Pulsed Laser Deposition**

Pulsed laser deposition, or PLD, is a physical vapor deposition process that is carried out in a vacuum system. A pulsed laser is focused onto a target containing the material to be deposited. For each pulse of the laser, a small amount of the target material, which is the bulk form of the material to be deposited, is vaporized or ablated, creating a plasma plume. The plasma plume then moves from the target to the substrate and deposits itself on the surface of the substrate [5]. A schematic of the process is shown in Figure 3. The deposition rate per laser pulse can range from 0.001 to 1 Å under typical conditions; this thickness depends on target – substrate separation, background gas pressure, and laser spot size [5]. In order to maintain uniform film thickness over large areas, it is necessary to manipulate the plume – substrate position. One common approach to overcoming this limitation is to combine substrate rotation with rastering of the ablation beam over a large ablation target [5].

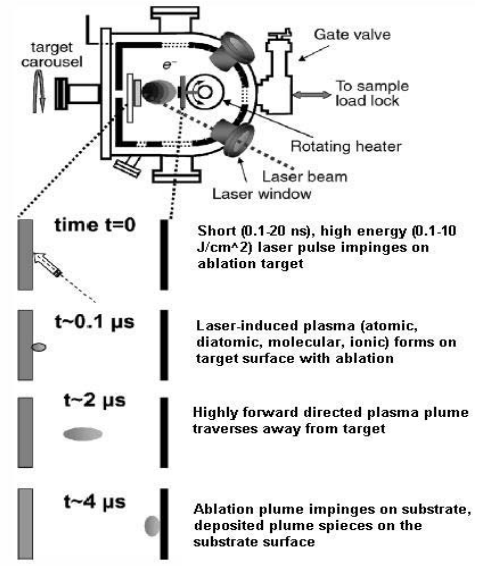


**Figure 3. Schematic of the PLD process [5].**

The dependence of film characteristics as a function of substrate temperature during growth is of great concern, as this thesis examines $HfO_2$ grown at substrate temperatures of 300°C, 500°C, and 750°C. As temperature is increased, the atoms, on hitting the substrate, will move and begin to agglomerate, often leaving voids in the film. Increased surface diffusion at the higher substrate temperatures, will often cause voids to be filled that would not normally be filled at the lower substrate temperatures, thus leading to a change in film quality and its crystal structure [6].

**Atomic Layer Deposition**

Atomic layer deposition (ALD) is a gas-phase thin-film deposition technique; it is a self-limiting growth method, which allows for highly uniform film thickness and composition [7]. As shown in Figure 4, each deposition cycle consists of four steps: (1) an exposure to a metal precursor, (2) a purge period, (3) an exposure to an oxygen precursor, and (4) another purge period [7]. The purge (or evacuation) periods are necessary to remove the non-reacted precursors and the gaseous reaction by-products [7]. The four-step cycle continues until the desired thickness is achieved. Film quality is heavily dependent on substrate temperature, as well as precursor and oxidant pressure, reactivity, and time in chamber [7]. The specific details of $HfO_2$ ALD sample growth will be discussed in the Methodology section.

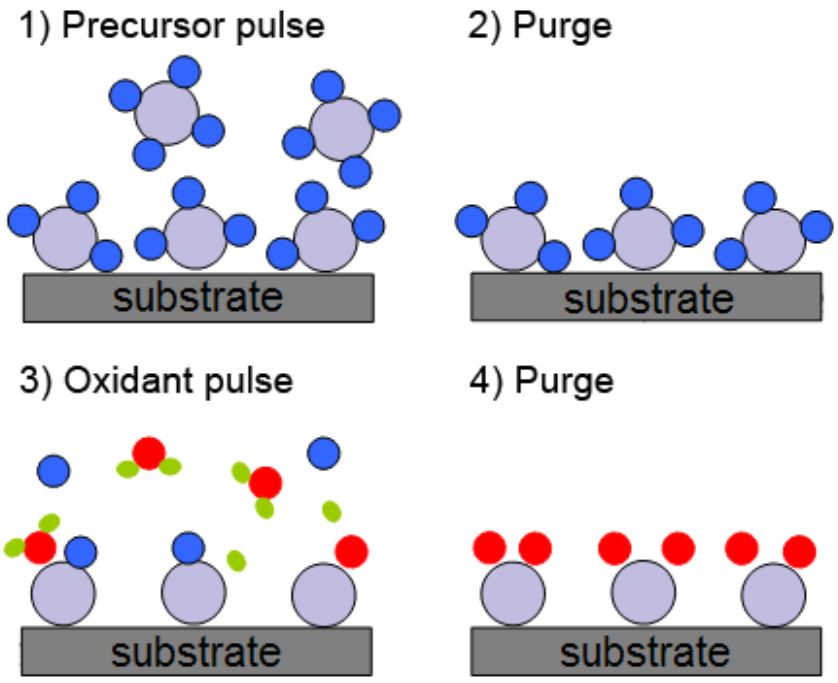


**Figure 4. Schematic of sample growth using atomic layer deposition. The four stages of the cycle are shown [7].**

## Radiation

Unless otherwise noted, this section is extracted from information contained in Dr. Petrosky's *Radiation Effects on Electronic Devices* [7]. In simple terms, radiation is any process in which energetic waves or particles travel through a medium, and is broken down into two categories: ionizing and non-ionizing. Ionizing radiation can either create an e-h pair or remove an electron from the atom, which is called atomic ionization. In atomic ionization, the freed electrons can then travel through the material and ionize further. Non-ionizing radiation can be divided into two categories: elastic and nuclear. In an elastic interaction, the radiation deposits enough energy to displace an atom from its lattice site, which can result in the production of a point defect. In nuclear absorption, radiation that is not charged (e.g. a neutron) can be absorbed into the nucleus, thus

causing it to become unstable or, depending on its energy, displace atoms in the irradiated sample.

This thesis will focus on the three particles used to irradiate $HfO_2$: gamma particles (photons), heavy ions (charged particles), and neutrons (uncharged particles). Both gamma particles and heavy ions are primarily ionizing, and neutrons are primarily non-ionizing. Both heavy ions and neutrons can cause atomic displacements.

Photons will interact with the material through the photoelectric effect, Compton scattering, and pair production; all interactions produce energetic free electrons. In the photoelectric process, the energy of the incident photon is completely absorbed by the emitted electron, either emitting a characteristic X-ray or a low-energy Auger electron, depending on the Z value. In Compton scattering, the photon energy is much greater than the binding energy of the atomic electron, creating an energetic Compton electron and a lower-energy photon which continues to travel in the material. In pair production, a photon striking the material will be completely absorbed and cause a positron-electron pair to form; a positron is identical to an electron in all ways except it has a positive charge. Figure 5 illustrates the dominant photon interaction as a function of incident photon energy and atomic number (Z) of the target material. The atomic number of hafnium is 72 and the atomic number of oxygen is 8, yielding an effective atomic number of 67.26 for $HfO_2$ by the following equations [8]:

$$Z_{eff} = \sqrt[2.94]{f_1 \cdot Z_1^{2.94} + \ldots + f_n \cdot Z_n^{2.94}} \tag{2.2}$$

$$f_n = \frac{Z_n}{\sum_{n=1}^{N} Z_n}. \tag{2.3}$$

For $HfO_2$, $Z_{eff} = \sqrt[2.94]{\frac{72}{72+8+8}72^{2.94} + \frac{8}{72+8+8}8^{2.94} + \frac{8}{72+8+8}8^{2.94}} = 67.26$. According to Figure 5, the photoelectric effect will dominate up to a photon energy of about 0.5 MeV and pair production will dominate above a photon energy of about 5 MeV, with Compton scattering taking precedence over the intervening photon energies.

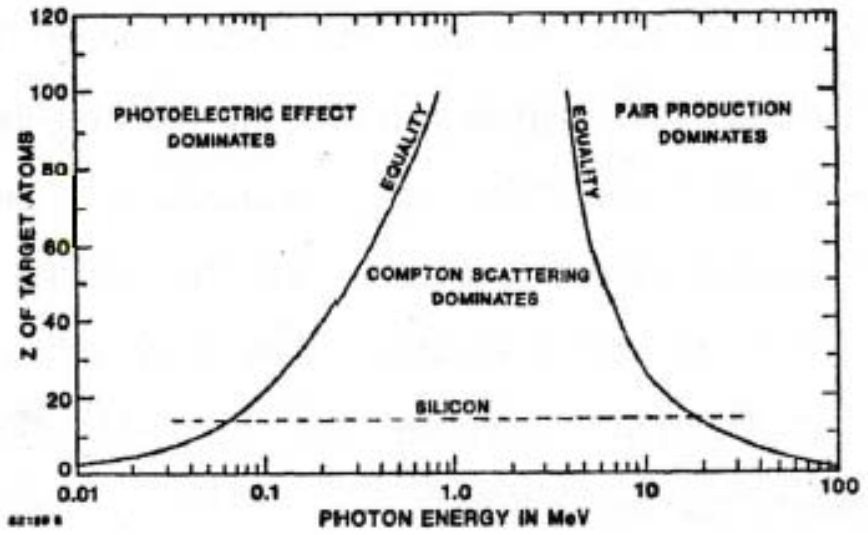


**Figure 5. Photon interaction mechanisms as a function of photon energy and Z of material [7].**

Charged particles will primarily interact by Rutherford scattering when incident upon the target material, which can cause both excitation and ionization of atomic electrons. Additionally, charged particles with sufficient energy can interact with the nucleus of the atom, which will be explained further for uncharged particles.

Uncharged particles can interact with the material in two ways: scattering and absorption. Neutron scattering, like photon scattering, will decrease the energy of the neutron and transfer some of its energy to the nucleus with which it collides. The absorption process with uncharged particles, like photon absorption (photoelectric effect) will pass all energy from the neutron to an alpha particle, beta particle, gamma particle, proton, or more new neutrons, depending on the binding energy of the added neutron and the kinetic energy of the captured neutron.

All this knowledge of radiation then begs the question as to what this damage will do to the material in terms of its CL spectrum. The damage to the material will either be in the form of ionization damage or displacement damage [9]. Ionization damage is the dominant mechanism when energetic photons (e.g. gamma rays) interact with the material [9]. Gamma rays are not expected to produce any permanent damage in the material as the particles are not displacing any atoms, but for $E_{ph} > 170$ keV, energetic backscattered Compton electrons may cause damage to the lattice [9]. The stopping power of the material may be determined by the following equation:

$$-\frac{dE}{dx} = 2Pq^4 Z_1^2 Z_2 N_{at} \frac{M_2}{m} \frac{1}{E} \ln\left(\frac{4E}{E_{eh}}\right) \tag{2.4}$$

where $Z_1$ and $Z_2$ are the atomic charges of the incident particle and the target material, $N_{at}$ is the atomic density of the target, $M_2$ is the corresponding atomic mass, $m$ and $E$ are the mass and energy of the incident particles and $E_{eh}$ is the mean ionization energy [9]. The amount of energy deposited in the material through ionizing interactions is determined by the Linear Energy Transfer function,

$$\rho_m^{-1} dE / dx \text{ [MeV cm}^2\text{/g]}, \quad (2.5)$$

where $\rho_m$ is the density of the material [9].

Ions, though, can cause displacement damage and thus change the CL spectrum of the material when examining the location where the damage occurred. If a new isotope created by the addition of a neutron is unstable and decays by particle emission, then the electrical and chemical properties of the material are likely to be changed, which may lead to changes in the CL spectrum of the material as well. Kucheyev et al. found that relatively low-dose keV light-ion bombardment (corresponding to the generation of ~$5 \times 10^{19}$ vacancies/cm$^3$) of wurtzite GaN resulted in a dramatic quenching of visible CL emission, but no comments were made as to any change in shape of the spectra [10]. Additionally, displacement damage occurring at room temperature may cause primary defects to migrate; this may result in defects disappearing by recombination at the substrate or by becoming trapped by impurity atoms [9].

**Optical Processes**

When light interacts with a material, it can experience three general phenomena: reflection, propagation, and transmission. The amount of light transmitted is related to the reflectivity of the material and the way the light propagates through the material. During propagation, there are then four more phenomena that can occur: refraction, absorption, luminescence, and scattering. Refraction reduces the speed of light from its speed in free space, represented by the constant *c*, to a new velocity, $v = c / n$ where *n* is the index of refraction. Index of refraction can furthermore be related to the relative dielectric constant of the material by Maxwell's equations, giving

$$n = \sqrt{\varepsilon_r}\ . \tag{2.6}$$

(The tilde denotes that the value is complex, with $n = n_R + in_I$ and $\varepsilon_r = \varepsilon_1 + i\varepsilon_2$.) [11]

Absorption occurs when the frequency of the light is resonant with the transition frequencies of the atoms in the medium, attenuating the beam; the absorption coefficient is given by

$$\alpha = \frac{4\pi n_I}{\lambda}, \tag{2.7}$$

where λ is the vacuum wavelength of the light [11].

Luminescence is the general term for the spontaneous emission of light by excited atoms in a solid-state material. The atoms can be excited in many ways, not only by the absorption of light (photoluminescence), but also by the absorption of heat (thermoluminescence) , electrical current (electrical luminescence), or an electron beam (cathodoluminescence), for example. It should be noted that all energy absorbed, no matter the form, will not necessarily result in luminescence if the excited atoms dissipate the energy as heat before the luminescence can occur [11].

Finally, light interacting with the medium will scatter, or change directions (and possibly frequency); this leaves the number of photons unchanged, but the number continuing in the initial direction will be decreased, thus attenuating the light. If the light frequency of the photon does not change, the scattering is elastic, and if the frequency does change, the scattering is inelastic [11]. The only phenomenon of interest in this thesis is that of luminescence, and more specifically cathodoluminescence, which will now be discussed.

## Cathodoluminescent Theory

Cathodoluminescence (CL) is a phenomenon in which a beam of electrons**,** generated by an electron gun, is incident upon a material, causing the material to luminesce through the excitation of its electrons by the beam's current. Figure 6 gives a basic diagram of CL. The emitted light will have various features, or peaks, at wavelengths correlating to the band gap and impurity transitions, as illustrated in Figure 7. The purpose of CL is to determine the optical properties, composition, and quality of the material of interest. Depth-resolved studies using CL can also be performed, which are beneficial in the study of radiation damage, since damage may not have occurred uniformly across the entire thickness of the material.

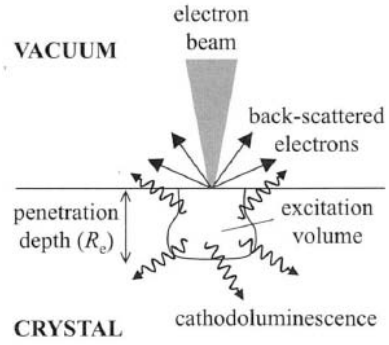


**Figure 6. Generation of cathodoluminescence following excitation of a crystal by an electron beam [11].**

Figure 7 presents all transitions possible in a material, but all these transitions will not necessarily be seen by CL. Due to its nature, CL only collects information on the radiative transitions in a material, so group (3) of the figure will never be present in a CL spectrum. Additionally, although we probably won't see any donor-acceptor pair (impurity-impurity) transitions, we do expect to see band-impurity and band-defect transitions. For example, some authors have attributed certain peaks in the $HfO_2$ spectra

to oxygen vacancies, which would present themselves as band-to-defect transitions. A material is considered to have a wide band gap when the band gap energy is larger than 1.7 eV; $HfO_2$, with a band gap energy of approximately 5.9 eV, has a large band gap, which makes it an insulator.

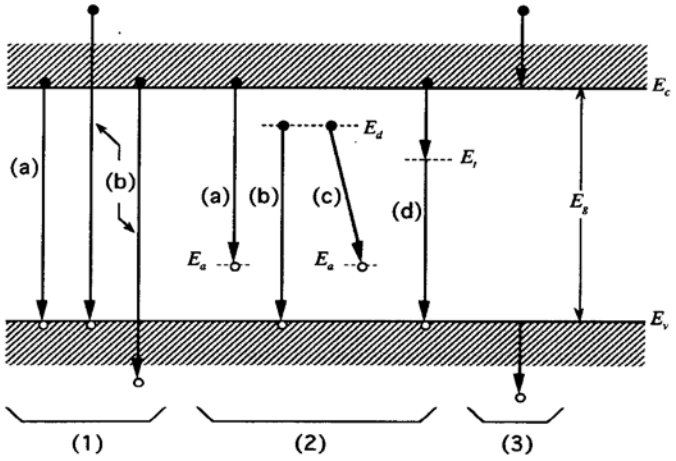


**Figure 7. Possible energy transitions in a semiconductor. $E_c$ is the energy of the conduction band, $E_v$ is the energy of the valence band, $E_g$ is the band gap energy, $E_d$ is the energy of the donor (impurity) level, and $E_a$ is the energy of the acceptor (impurity) level. Group 1 represents band-to-band transitions, group 2 represents impurity transitions, and group 3 represents non-radiative transitions, which cannot be observed using CL; these transitions will only be considered when trying to minimize them.**

High-energy electrons penetrating the surface of the material will transfer their energy to the crystal by causing electrons in the valence band of the material to be excited to the conduction band, which results in the creation of e-h pairs [11]. The electrons then fall from their high energy state to a lower energy state in a different group of levels in a process called recombination, which releases energy in the form of phonons or photons. The energy (frequency/wavelength) of the emitted photon depends on the material's band gap and impurities, as well as the type of recombination occurring. The number of e-h pairs generated per primary electron is given by:

$$N^{eh} = (1-\gamma)\frac{E^p}{E^i}, \tag{2.8}$$

where γ is the fractional energy loss due to back scattering, $E^p$ is the energy of the primary electron, and $E^i$ is the ionization energy (i.e., the energy required to form an e-h pair) [11]. $E^i$ can be calculated using the semi-empirical formula:

$$E^i = 2.8E_g + E', \tag{2.9}$$

where $E'$ depends only on the material and has a magnitude in the range of 0-1 eV [11]. Pair production is actually a multi-step process that also involves re-emission and subsequent inelastic scattering of secondary electrons, but for many materials, equation (2.9) is sufficient. Therefore, given a beam energy of 5 keV and assuming $E' = 0.5\,\text{eV}$ for $HfO_2$, whose band gap is 5.9 eV, each electron incident on the material will produce several hundred e-h pairs. For smaller band gap materials, the $N^{eh}$ will become larger because it is easier to excite electrons across the band gap.

It is beneficial to use CL over other luminescent processes such as photoluminescence (PL) because PL requires a light source, usually a laser, with high enough energy to excite electrons across the band gap. Such lasers are not always easy to obtain for wide bandgap materials such as $HfO_2$. Additionally, PL does not allow for depth-resolved studies of materials.

**Penetration Depth for Electrons**

As was stated above, it is possible to excite luminescence from different depths of a material by varying the electron beam energy [12]. Since this thesis is concerned with analyzing damage caused by radiation, it is desirable to consider the specific depths at

which any damage may have occurred. (SRIM software was used to determine the depth of the damage, which will be discussed later.) To determine the depth being probed by a given energy, the CASINO V2.42 Monte Carlo simulation program was used. Unless otherwise noted, the information in this section is adapted from D. Drouin et al.: CASINO 2.42 [13].

The following description of the calculated electron trajectories is based on the default physical models, though the program has several models preprogrammed. CASINO assumes a Gaussian-shaped electron beam, with the beam diameter being chosen by the user. The distance between two successive collisions is evaluated using the equations

$$L = -\lambda_{el} \log(R_4) \text{ [nm]} \tag{2.10}$$

$$\frac{1}{\lambda_{el}} = \rho N_0 \sum_{i=1}^{n} \frac{C_i \sigma_{el}^i}{A_i} \tag{2.11}$$

where $C_i$, $A_i$, are the weight fraction and atomic weight of element $i$, respectively, ρ is the density of the region in $g/cm^3$, and $N_0$ is Avogadro's number. $R_4$ is a random number uniformly distributed between 0 and 1. The value of the total cross section, $\sigma_i$ ($nm^2$), for each chemical element is determined using the pre-calculated and tabulated value [14].

The program neglects the effect of inelastic scattering on electron deviation; it also groups all the electron energy loss events in a continuous energy loss function [15]. Energy is then calculated using the following equations:

$$E_{i+1} = E_i + \frac{dE}{dS} L\,, \tag{2.12}$$

$$\frac{dE}{dS} = \frac{-7.85\times10^{-3}\rho}{E_i}\sum_{j=1}^{n}\frac{C_j Z_j}{F_j}\ln\left(1.116\left(\frac{E_i}{J_j}+k_j\right)\right), \tag{2.13}$$

where $Z_j$ and $J_j$ are atomic number and mean ionization potential of element $j$, respectively. $K_j$ is a variable whose value only depends on $Z_j$ and is always close to but less than unity [16]. The actual penetration depth of the electrons uses an equation derived by Kanaya and Okayama in 1972,

$$R_e = \left(27.6A/\rho Z^{0.889}\right)E_b^{1.67}, \tag{2.14}$$

where $A$ is the atomic weight [g/mol], ρ is the atomic density [g/cm$^3$], $Z$ is the atomic number, and $E_b$ is the energy of the beam. In examining hafnium dioxide with a beam energy of 5 keV,

$$R_e = \left(27.6\times210.4888/9.68/67.26^{0.889}\right)5^{1.67} = 209.25\,[\text{nm}]. \tag{2.15}$$

The figure below shows a sample excitation volume generated by a 5 keV electron beam in 50 nm thick $HfO_2$. The penetration depth is also presented in the figure.

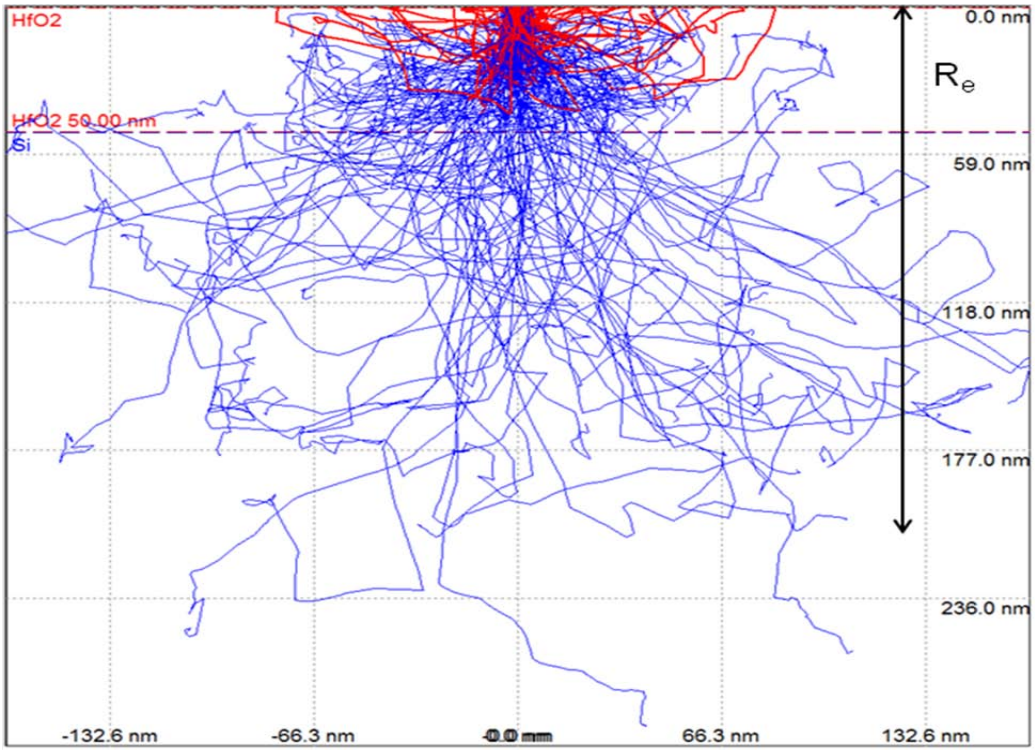


**Figure 8. Sample Monte Carlo simulation using an electron beam energy of 5 keV and a sample of $HfO_2$ that is 50 nm thick with a density of 9.68 g/cm$^3$. The arrow indicates the calculated penetration depth, $R_e$, given by equation (2.15) and also illustrated in Figure 6.**

## Relevant Research

Ito *et al.*, 2005, studied PLD $HfO_2$ using PL with the spectra induced by ultraviolet photons. The sample was amorphous and deposited on $SiO_2$ to a thickness of $1.1\times10^3$ nm [17]. The stoichiometry actually found the sample to be oxygen deficient, with the actual composition giving $HfO_{1.10}$. They also studied amorphous $HfO_2$ on Si grown by plasma-enhanced chemical-vapor deposition (PECVD), also oxygen deficient and much thinner (88 nm and 130 nm). Elemental composition was determined by x-ray photoelectron spectroscopy (XPS). Their results showed consistent peaks at 2.8 eV and 4.2 eV (after annealing at 900°C in oxygen), or 4427 Å and 2951 Å, respectively. Because the PL spectra do not reflect the large differences in oxygen content of the

samples, the peaks cannot be due to oxygen vacancies. Experiments were also conducted comparing the samples to the new PECVD samples deposited on $CaF_2$ crystal plates as substrates with no change in PL, indicating that the features cannot be due to defects at the interface. Likewise, the features cannot be caused by impurities due to the improbability of all samples possessing the same impurities in the same percentages. These two features must then be intrinsic to $HfO_2$. They attribute the 2.8 eV feature to radiative recombination between localized states in the band tails, while the 4.2 eV feature is excited due to the interband absorption.

Strzhemechny *et al.*, 2008, studied $HfO_2$ grown by PECVD to a thickness of approximately 100 nm [18]. Low energy electron-excited nanoscale (LEEN) luminescence spectroscopy found optical transitions at 2.7, 3.4, 4.2, and 5.5 eV which they have assigned to defect-associated radiative transitions. These 2.7 and 4.2 eV features agree with the findings Ito *et al.*

Mendoza *et al.*, 2010, studied $HfO_2$ films deposited by ultrasonic spray pyrolysis process on corning glass substrates at temperatures of 300, 400, 500, and 600°C [19]. They found the films to be amorphous for substrate temperatures below 400°C and monoclinic for substrate temperatures higher than 450°C. PL studies showed a consistent peak at 4250 Å (2.9 eV) when excited with a 2540 Å light source. For the two monoclinic samples (500 and 600°C), peaks also appear at 5120 and 6500 Å, or 2.42 and 1.91 eV. The peak at 2.9 eV matches well with Strzhemechny's 2.7 eV peak and Ito's 2.8 eV peak. After performing electron dispersive spectroscopy (EDS), it was determined that all samples contain considerable amounts of chlorine, whose presence is cited as the source of the 4250 Å peak. They attribute the two other features to radiative recombination at

impurity and/or defect centers. Deep levels related to oxygen vacancies could theoretically contribute to emission at these wavelengths; obviously recombination of photoexcited electron-hole pairs (excitons) captured by those centers lead to the PL emission.

Zhao *et al.* study $HfO_2$ using local-density approximation (LDA) and the generalized gradient approximation [1]. Though no mention is given to the thickness, deposition method, or substrate material, or substrate temperature, they state that $HfO_2$ is monoclinic at low temperature, tetragonal at higher temperatures, and then cubic at even higher temperatures; unfortunately, there is no delineation of temperature ranges over which these structures occur.

Cheynet *et al.*,2007, have further determined that $HfO_2$ can form in an orthorhombic structure, using both ALD and chemical vapor deposition (CVD) as the growth methods [2]. The thin films were grown on Si (001).

Mendoza *et al.* also present a study of XRD intensity of $HfO_2$ at all four sample temperatures. Based on the shape, the samples were determined to be either amorphous or monoclinic, as previously stated. Figure 9 illustrates this XRD pattern. Smirnova *et al.* present a similar plot for monoclinic $HfO_2$ grown by metalorganic chemical vapor deposition (MOCVD) [20]. Wang *et al.* and Aarik *et al*. also agree with the monoclinic XRD findings; Wang also presents XRD spectra of the cubic phase of $HfO_2$ grown by PLD at substrate temperatures of 600 and 700°C [21] [22]. Based on this information, an attempt will be made to determine the structure of $HfO_2$ studied in this thesis, presented in the Chapter IV. Based on all the different growth methods used that achieved

monoclinic structure, it appears that structure is irrelevant of growth method with temperature appearing to be the deciding factor.

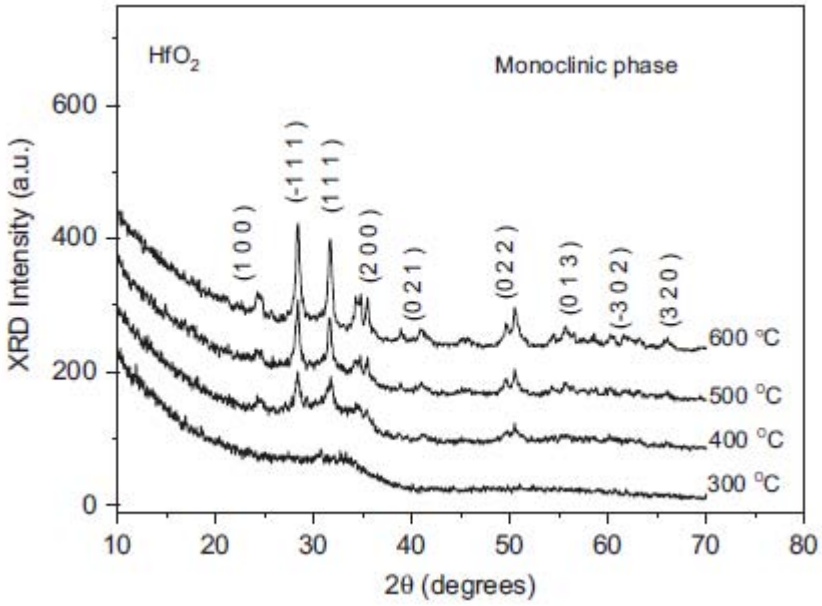


**Figure 9. XRD diffractograms for $HfO_2$ films grown at different $T_S$: 300, 400, 500, and 600°C**

While there is plenty of literature pertaining to the study of $HfO_2$ and its luminescence, there only exists a small amount of literature pertaining to its cathodoluminescent spectra. It was found that the spectra for any given $HfO_2$ sample is highly dependent upon the growth method and conditions, and any annealing that may have been done to the sample. Research found chemical vapor deposited (CVD) samples with peaks at 2.7, 3.7 and 4.0 eV, with a bandgap ranging anywhere from 4.2 to 6.8 eV, depending on the synthesis conditions [23]. ALD samples had peaks at 2, 2.5, 3.9, and 4.3 eV, and a pronounced doublet at 3.35 and 3.5 eV, with a bandgap at 5.9 eV [24]; however, these samples had 10 nm of Mo deposited on top of 4 nm of $HfO_2$.

Figure 10 (a) depicts the photoluminescence spectra of chemical vapor deposited (CVD) $HfO_2$ on a silicon *n*-type (100) substrate; since the researchers did not anneal the samples studied in this paper, the relevant portion of Figure 10 (a) is trace 1 [25]. The excitation source was a 400w hydrogen-deuterium filtered through a monochromator providing photons of energy 5.8 eV. The CVD samples were also examined using cathodoluminescence, which is depicted in Figure 10(b). Again, the as-deposited sample is the one relevant to this thesis, not the annealed sample.

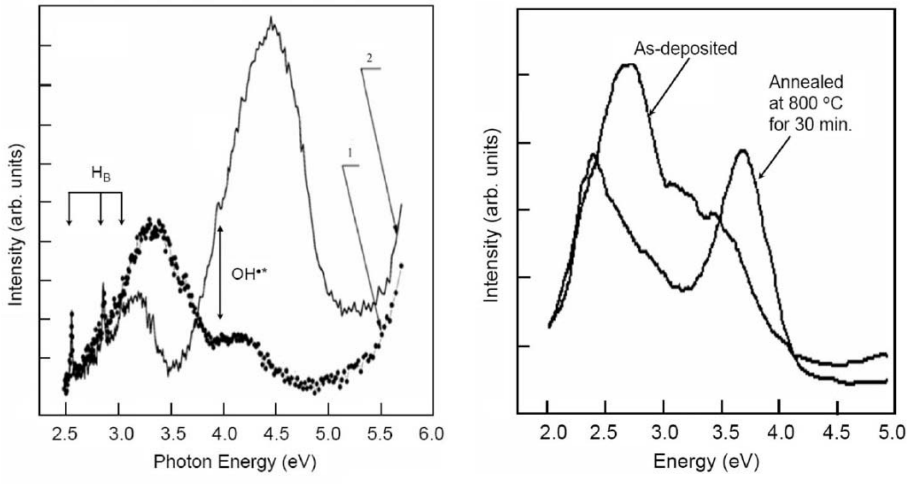


(a) (b)

**Figure 10. a) Photoluminescence spectra of 1030 Å thick $HfO_2$ grown at 973 K (spectrum 1) by ALD and annealed in air at T=1173 K (spectrum 2). The three vertical arrows point to the positions of the Balmer lines 2.550 eV, 2.856 eV, and 3.0226 eV from the source of light. Before annealing, peaks occur at 3.35 eV and 4.13 eV [25]. After annealing is not of interest as no annealing was done to the samples examined in this document. b) Cathodoluminescence spectra of as-deposited $HfO_2$ film and sample annealed at 800°C for 30 min; grown by chemical vapor deposition [23]. Peaks occur at 2.7 eV and 3.5 eV for the as-deposited sample.**

Figure 11 depicts samples of $HfO_2$ grown by ALD with varying substrate temperatures (500K, 770K, and 1200K) and measurement temperatures (10K and 295K); band-gap energy is 5.55±0.03 eV. An increase in temperature during measurements

found the excitation spectra shifted towards lower energies by 0.1 to 0.15 eV, which indicates a corresponding change in the band-gap energies.

It becomes apparent in Figure 11 that the emission spectra can change drastically between both growth conditions and measurement conditions; the change in the spectra between 10K and 295K sample temperatures is especially apparent in the 770K sample.

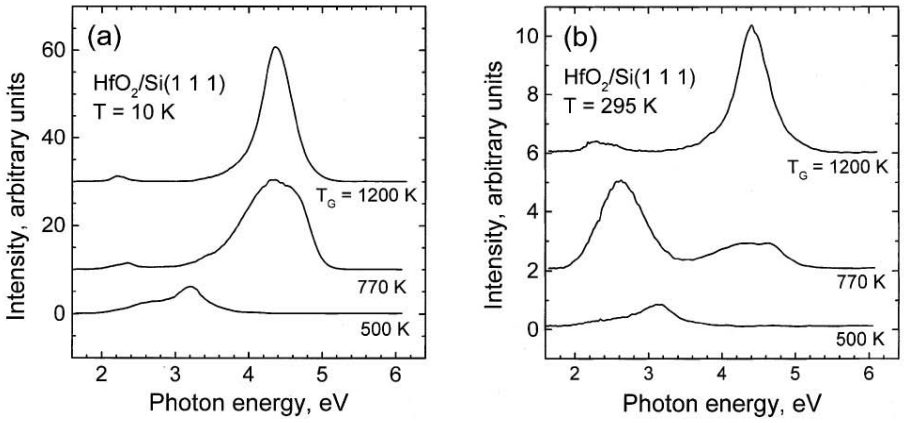


(a) (b)

**Figure 11. Photoluminescence emission spectra recorded at (a) 10K and (b) 295K; all samples examined were grown by ALD, with substrate temperatures labeled in the figures [22].**

# III. Methodology

## Chapter Overview

The purpose of this chapter is to explain the experimental setup used in CL, including calibration of the system and determining its total spectral response. Corrections to the raw data collected by the software will also be discussed. Finally, the samples used and the amount and type of radiation received will be addressed.

## Experimental Setup

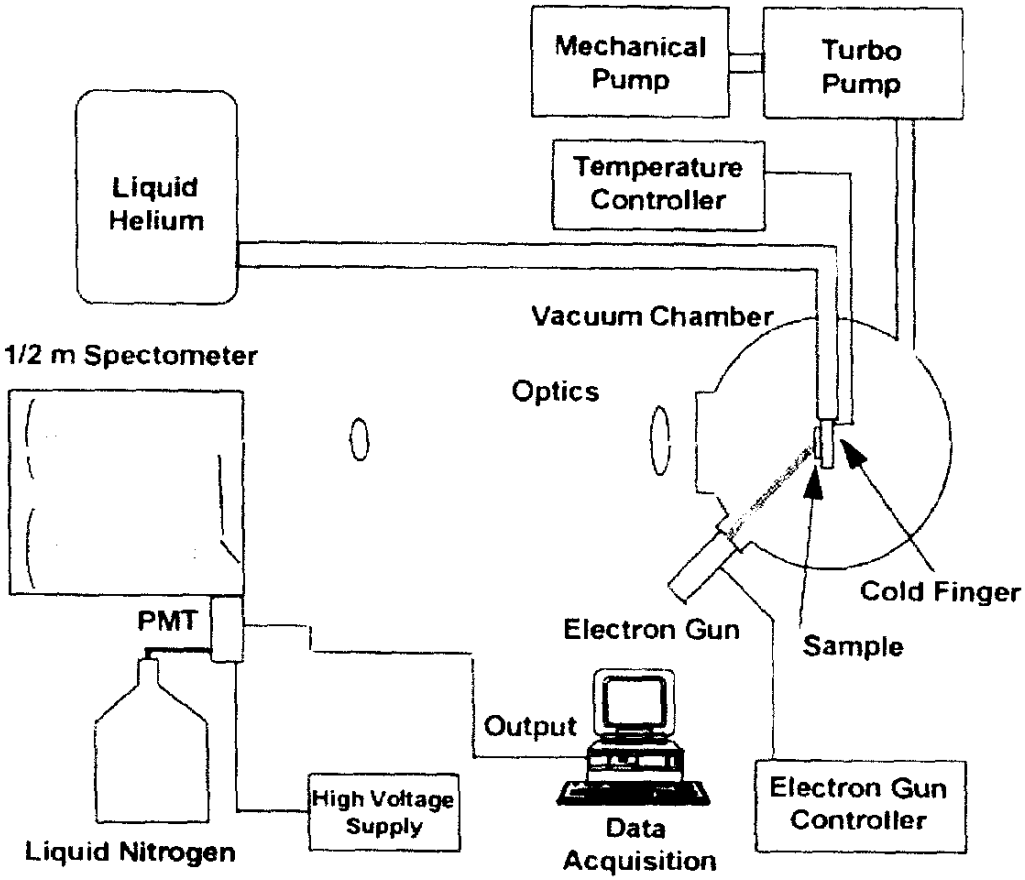


**Figure 12. CL setup [26].**

In cathodoluminescent spectroscopy, a sample material is placed inside a vacuum chamber and mounted on a sample holder, which may be cooled (as desired) by a liquid helium refrigerator. A temperature controller allows one to set the sample temperature to the desired value, ranging from approximately 7K to 300K, which provides for temperature dependent studies. Additionally, cooling the sample to 7K minimizes the thermal broadening effects and thus increases the signal-to-noise ratio and the intensity of the spectra collected [12]. The chamber is evacuated to a medium vacuum ($10^{-3}$ torr) by a mechanical (roughing) pump, and then evacuated to a high vacuum (~$5x10^{-7}$ torr) by a turbo pump. The electron gun, which is also in the vacuum chamber, excites the sample, causing it to emit light. The light is collected by a series of two optics, the first located outside the vacuum chamber and one focal length away from the sample and the second at one focal length away from the entrance slit of the spectrometer; the distance between the two optics should be kept small to minimize the amount of light scattered. The light is then sent through a grating spectrometer and finally a photomultiplier tube detector, which is cooled to -30°C to reduce the noise in the signal; Figure 13 shows data collected when the PMT is cooled and also at room temperature to emphasize the effect cooling has. Finally, the data are collected by the SynerJY data acquisition program, which yields intensity of the light as a function of wavelength. A diagram of the setup is given in Figure 12.

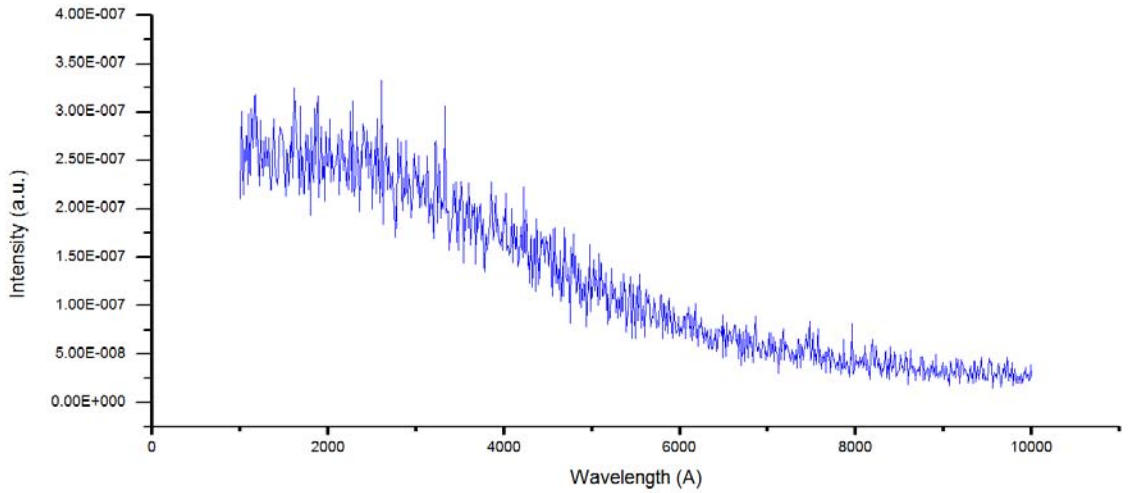


**Figure 13. Time-dependent plot of detector signal as temperature decreases from 25°C to -30°C, cooled by liquid nitrogen. No sample was present.**

## The Sample

Our samples, which are roughly 0.25 $cm^2$ in size, are mounted on the sample holder in the vacuum chamber using a very small amount of vacuum grease. The chamber is then evacuated to a pressure on the order of $10^{-7}$ torr, which is in the high vacuum (HV) range. This is necessary in order to keep the surface of the sample relatively clean. Additionally, HV is necessary to permit the use of our low energy electron gun without undue interference from gas phase scattering. The sample was examined at temperatures ranging from 7K to 300K, with the range being restricted by the limits of the equipment available.

There are many methods for growing materials, but the two types of samples studied will be those grown by either pulsed laser deposition or atomic layer deposition.

## Electron Gun

The Electron Gun is the source of the electron beam that is used to excite the material in the vacuum chamber. The gun and power supply used, model EMG-12/EGPS-12, were manufactured by Kimball Physics, with beam energy ranging from 100 eV to 20 keV and beam current ranging from 10 nA to 100 μA. The spot size ranges from 500 μm to 25 mm. Unless noted otherwise, the information in this section was taken from the Electron Gun's Instruction Manual. The elements comprising the gun are the triode, blanker, focus, and deflection, which produce and control the electron beam. The triode consists of a cathode, Wehnelt (grid), and anode. Each element is labeled below in Figure 14. Electrons are emitted from the cathode and accelerated to full kinetic energy (set by the operator) by the triode's electric field. The cathode, a thermionic emitter, is directly heated by an isolated voltage source and floated below ground with a negative high voltage supply, ranging from 0 to 20 kV. Electron emission depends on the cathode temperature and the grid voltage applied.

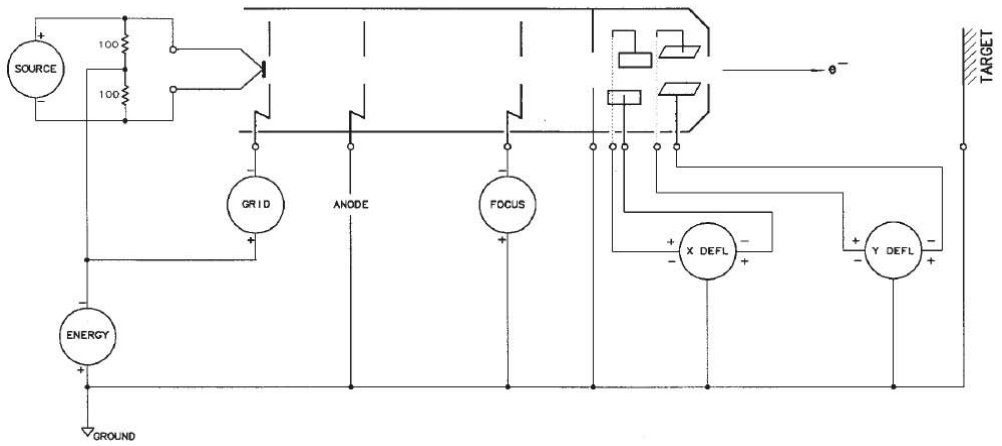


**Figure 14. Block diagram of Kimball Physics EMG-12 Electron Gun. The element labeled "G-1" is the Wehnelt (grid).**

The gun used for this study features a standard electron optical system utilizing a refractory metal thermionic emitter consisting of a small disk mounted on a hairpin filament wire. When the filament wire is heated by the voltage source, the disk provides a circular, planar emission surface that emits electrons.

The Wehnelt, or grid, is a tube-shaped structure with an opening fixed to one end that houses the cathode. In Figure 14, the Wehnelt is labeled as “G-1”. The Wehnelt potential is controlled by a voltage source referenced to the negative 0 to 10 kV energy supply. An increase in the Wehnelt potential makes the Wehnelt aperture more negative with respect to the cathode, and the electric field between the cathode and Wehnelt suppresses electron emission from the edge of the cathode, leaving only the center of the cathode to emit. A high enough Wehnelt potential will suppress the beam completely. Additionally, the electric field created by the Wehnelt also controls beam divergence by varying electron trajectories.

The anode is an aperture plate which is located downstream of the Wehnelt and is at ground potential. The potential difference between the anode and cathode (as modified by the Wehnelt potential) controls the magnitude and direction of the electric field, which determines the trajectory of the electrons emitted from the cathode. The beam energy does not change once it passes through the anode.

The focus elements consist of three tubes of equal diameter arranged in series. The first and third tubes are grounded while the second element is at focusing potential (kV). This type of lens is known as an Einzel lens, illustrated in Figure 15. The negative focusing potential controls the position of the beam’s second axial crossover point, which

allows the spot to be focused on a target placed at a wide range of distances (100 mm to 1000 mm); the higher the potential, the farther the crossover point will be, thus allowing the distance to the target to be farther as well. Ultimately, the goal is to set the focusing potential such that the beam is focused at the target (i.e. the second axial crossover point is located at the surface of the material). At a fixed target distance, the focus value needed for minimum spot size varies linearly with the energy of the beam.

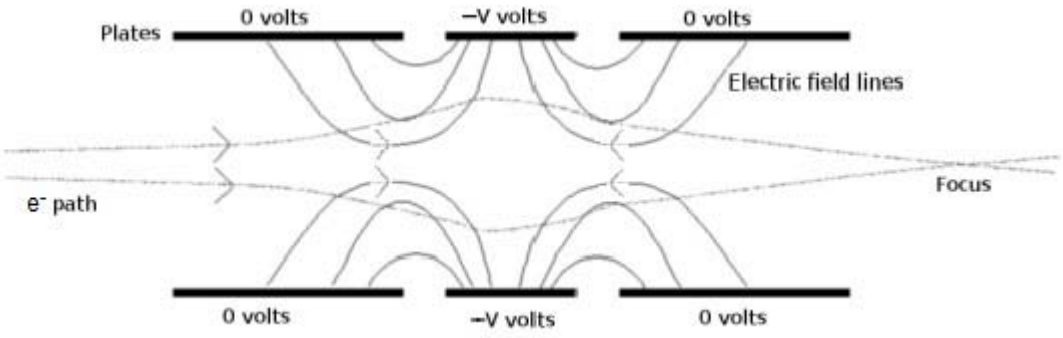


**Figure 15. Einzel lens diagram utilizing a negative focusing potential [27].**

Lastly, deflection consists of two pairs of deflection plates located downstream of the focus element, allowing for X and Y deflection. Independent potentials can be applied to each set of plates to provide a deflecting force perpendicular to the direction of travel of the electron beam. The beam can then be aimed at different locations inside the vacuum chamber depending on the location of the sample being examined. Distortion of the spot may occur if the beam is deflected too much (i.e. higher potential applied to the plates), due to the non-uniformities in the deflecting electric field that occur at the edges of the deflection plates. A larger beam passing through the deflection plates will be distorted more than a smaller beam. Ideally, the samples should be mounted in the chamber so as to minimize deflection needed, thus minimizing beam distortion.

In conducting studies to compare the excitation occurring in the material at different energies (i.e. different depths), the power should be held constant in order to maintain the same number of e-h pairs generated at each depth examined. Therefore, a decrease in beam energy should be accounted for by an increase in beam current. This thesis did not focus on keeping a constant power and therefore a constant intensity because intensity can only be expressed in terms of its change in relation to the shape of the spectra. This is due to the limitations in our ability to precisely control the size and location of the electron beam; therefore, beam current was held constant for most experiments while beam energy was varied (i.e. power was not held constant).

**Optical System**

The light that is emitted from the material is collected by an optical system consisting of two convex lenses before being sent into a grating spectrometer. The two lenses are necessary to focus the energy of the light; the more intensity collected by the spectrometer the lower the signal to noise ratio will be. The first lens is placed one focal length from the sample inside the chamber, thus collimating the light as it leaves the first lens. The second lens is placed one focal length from the grating spectrometer's entrance slit, which focuses the light onto the entrance slit. The distance between the two lenses is theoretically irrelevant, but in practice should be kept small to avoid any unnecessary loss of light due to defects in the lenses and improper alignment. It should be noted that the ideal alignment of the lenses will produce a spot on the entrance slit that uses as much of the slit as possible (as opposed to the traditional sense of the word "focus" that implies all the light is focused to a single point).

## Grating Spectrometer

The grating spectrometer used in this experiment is a Spex 500M grating spectrometer. The grating used is a Horiba JY plane ruled grating blazed at 330 nm with 1200 grooves/mm at a blaze angle of 10.4°. The length is 0.5 m. The purpose of the grating spectrometer is to allow for the intensity of the light to be measured as a function of wavelength. The efficiency of the grating decreases as one measures wavelengths farther from the blaze wavelength and thus the raw intensity collected is not entirely accurate representative of true sample spectrum.

## Photomultiplier Tube

After the light passes through the spectrometer, it arrives at the photomultiplier tube (PMT), which converts the photons to electrons by the photoelectric effect. The PMT used is an RCA C-31034-02 PMT with a gallium arsenide (GaAs) photocathode; it was set to a bias of -1200V for all experiments. The PMT was cooled to -30°C using liquid nitrogen. Due to the nature of light, there is inherent randomness in the signal collected, creating noise. The photocathode was designed to have a low work function, $\varphi$, in order to allow longer wavelengths of light to be detected, but this also allows thermionic emission, which further increases the noise in the signal. As the PMT is cooled, the Fermi level shifts down and thermal electrons are removed, thus giving a less noisy spectrum. Figure 16 illustrates the spectral responsivity of the PMT as a function of wavelength in nm; the PMT has a maximum quantum efficiency of 20%.

The thermionic emission can be modeled by Richardson's equation, which states

$$J = A_G T^2 e^{-\phi/k_B T}, \tag{3.1}$$

$$A_G = \lambda_R A_0, \tag{3.2}$$

$$A_0 = \frac{4\pi m k_B^2 e}{h^3}, \tag{3.3}$$

where $J$ is the emission current density in A/m$^2$, $A_G$ is Richardson's constant in A/m$^2$K$^2$, $T$ is temperature in Kelvins, $\phi$ is the work function of the photocathode (GaAs, in this case) in Joules, $k_B$ is Boltzmann's constant, $m$ is the mass of an electron, $e$ is the electron charge, and $h$ is Planck's constant, and $\lambda_R$ is a material-specific correction factor that is typically on the order of 0.5. The value of $A_0$ is $1.20173 \times 10^6$ A/m$^2$K$^2$. For a fixed work function, lowering the temperature reduces both the $T^2$ term and the exponential containing the -1/$T$ term, and thus a lower temperature will decrease the thermionic emission current density, $J$, which reduces the noise in the signal.

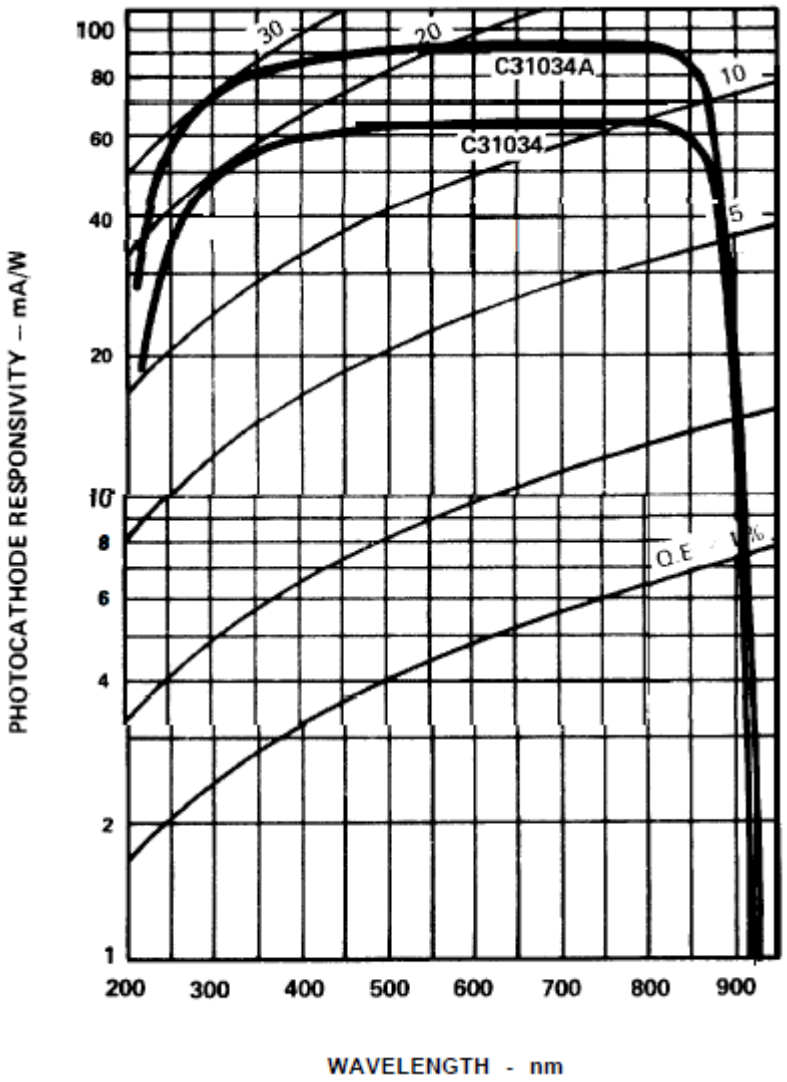


**Figure 16. RCA C-31034-02 PMT. Possesses a maximum quantum efficiency of 20%. Highly consistent responsivity over the 350-800 nm range.**

## Data Acquisition

The collected data were analyzed using the SynerJY data acquisition software provided by Horiba JY. This program provides the material's luminescent intensity as a function of wavelength in angstroms. In this program, it is possible to choose the step size of the wavelength measurements and the integration time at each wavelength. The step size should be chosen to be smaller than the resolution of the spectrometer, which

was determined to be approximately 16 Å/mm; for example, a step size of 5 Å should be sufficient when the slits are set to 1 mm, while a step size of 0.1 Å would not add any information to the spectrum. The integration time will affect the signal to noise ratio of the spectra. Because of the randomness in the signal, the spectra may show non-continuous intensities, making the plot look more jagged than smooth. As the integration time is increased, the randomness is averaged out and creates a smoother curve with more continuous intensities. It should again be noted that this raw intensity needs to be corrected for system response, i.e. the photomultiplier and the grating. The PMT was already shown to have a non-uniform spectral responsivity, and the grating used will further affect the intensity displayed, depending on the type, blaze wavelength, groove density, and blaze angle. These non-uniformities must now be corrected for via a calibration of the system against a calibrated standard such as a blackbody. In addition, the spectrometer wavelengths must be calibrated against a wavelength standard such as a spectral lamp.

**Wavelength Calibration**

Wavelength calibration of the system was done using an Oriel mercury calibration lamp. The peak values were obtained from the raw data and compared to Oriel's published mercury spectrum. As shown in Table 1, there is a consistent shift to a higher wavelength than expected, with the maximum wavelength error found to be 1.4 Å and an average error of 0.8 Å. Taking the derivative of energy as a function of wavelength and using the average error as $d\lambda$, error in energy at 2000 Å is approximately -0.00248 eV and -0.00020 eV at 7000 Å. Normally, linear regression would be performed to convert

the measured wavelength to the proper wavelength; this is necessary when dealing with narrow, well-defined peaks. When the data in question contain broad peaks, though, this small calibration error is less than the judgmental error and can thus be ignored. One could then argue that Gaussian curves should be fitted to the data to remove judgmental error, but there is also judgmental error associated with choosing the number of features present as well as the location of those features in order to fit multiple Gaussians to the data.

**Table 1. Peak wavelengths as measured by the equipment versus the theoretical wavelengths quoted by Oriel for their mercury calibration lamp. Data were collected using a 15 micron slit.**

| Measured (Å) | Actual (Å) | Difference (Å) |
|---|---|---|
| 2482.8 | 2482 | 0.8 |
| 2652.6 | 2652 | 0.6 |
| 2753.8 | 2752.8 | 1 |
| 2804.4 | 2803.5 | 0.9 |
| 2894.1 | 2893.6 | 0.5 |
| 2968.7 | 2967.3 | 1.4 |
| 3021.9 | 3021.5 | 0.4 |
| 3342.4 | 3341.5 | 0.9 |
| 3655.5 | 3654.8 | 0.7 |
| 3664 | 3663.3 | 0.7 |
| 4359.1 | 4358.4 | 0.7 |
| 5461.7 | 5460.7 | 1 |
| 5770.4 | 5769.6 | 0.8 |
| 5791.7 | 5790.7 | 1 |

The spectral response of the system (combined effects from grating spectrometer and photomultiplier tube) will be discussed in the results section.

**Pulsed Laser Deposition Samples**

The PLD $HfO_2$ samples were obtained from the University of Nebraska-Lincoln. $HfO_2$ was deposited on n-type silicon (100) substrates. There are six separate batches of PLD samples, with two batches each at substrate temperatures of 300°C, 500°C, and 750°C. The batches at each temperature are referred to as "thick" or "thin", though most of the thicknesses are not known (Rutherford Backscattering was performed on samples from two thin batches). The collection of PLD samples along with their radiation treatment is outlined in Table 2 below.

**Table 2. $HfO_2$ PLD samples obtained.**

| | | Irradiation Method | | | |
|---|---|---|---|---|---|
| PLD Sample Batch | Thickness[b] (nm) | Unirradiated | Gamma[d] | Gamma/Neutron[d] | Ion[d] |
| 300[a] thin | | X | | X[c] | X |
| 300[a] thick | | | X[c] | | |
| 500[a] thin | 82.45 | | X | X[c] | X |
| 500[a] thick | | X | | | |
| 750[a] thin | 148.1 | X | X | X[c] | X |
| 750[a] thick | | X | | | |

[a] This number refers to the temperature of the substrate during growth.
[b] Thickness, if known, was measured using Rutherford backscattering spectrometry with 2 MeV helium ions.
[c] It is not explicitly known if these samples are from the thin or thick batch at the temperature given.
[d] Specific doses and methods will be outlined below.

**Atomic Layer Deposition Sample**

The ALD samples of $HfO_2$ used were obtained from the Air Force Research Laboratory (AFRL) Sensors Directorate. The samples were deposited using a Cambridge NanoTech Fiji F200 ALD research and development system. The pressure in the chamber was nominally 0.19 torr with a standard deviation of 0.007 torr. The samples were deposited on a p-type silicon substrate at a temperature of 250°C; the samples were not annealed. The $HfO_2$ precursor was tetrakis(dimethylamido)hafnium(IV) or $(Hf[N(CH_3)_2]_4)_2$. It should be noted that the samples were all grown in one large piece and then cut into smaller pieces to be irradiated and tested as necessary. Table 3 outlines the different ALD samples that were examined.

**Table 3. $HfO_2$ ALD samples obtained.**

| $HfO_2$ ALD Sample Number | Thickness (nm) | Ion Irradiation[a] Fluence ($cm^{-2}$) |
|---|---|---|
| #1 | 50 | Unirradiated |
| #2 | 50 | 1E8 |
| #3 | 50 | 1E9 |
| #4 | 50 | 5E10 |

[a] Ionizing radiation was achieved using $^{+}1$ nitrogen ions at 20 keV.

**Radiation Doses**

All of the samples studied for radiation damage were irradiated by Captain Jesse Foster; gamma irradiation of PLD samples was done at the Gamma Irradiation Facility (GIF) at the Ohio State University Nuclear Reactor Laboratory (OSU NRL) using $^{60}Co$. The samples remained in the chamber for 140 minutes and received a total dose of 1 Mrad(Si). The error associated with this dose is less than 4%, as quoted by Captain

Foster. All dose levels (gamma, neutron, and ion) were chosen to mimic those used to study $SiO_2$.

All neutron irradiation of PLD samples was done at the Ohio State University Research Reactor (OSURR), which is a uranium reactor. The samples remained in the reactor for 2 hours at a reactor power of 450 kW and received a total dose of 25 krad (Si), which is the 1 MeV equivalent dose. The 1 MeV equivalent (1 MeV (eq)) neutron fluence is the fluence required of 1 MeV mono-energetic neutrons to cause the same amount of damage as the entire neutron spectrum for a given material. We want to know the total dose of silicon, not uranium, so the equivalent fluence must be calculated. Furthermore, the fluence must be converted to dose by a fluence-to-dose conversion factor, determined to be $3\times10^{-11}$ [rad(Si)cm$^2$]. There is an uncertainty associated with this dose of ~25% of the stated value. This uncertainty comes from two things: the uncertainty associated with obtaining the neutron spectrum using activation analysis, and the time the sample spent in the reactor before the power reached 100% (450 kW), which normally takes roughly 20-30 minutes.

Ion irradiation of PLD samples was done at the Ion Beam Laboratory (IBL) located at Sandia National Laboratory (SNL) using 1 MeV silicon ions in the $^{+}1$ charge state. The total dose (utilizing a TRIM simulation to determine $\partial E / \partial x$ in eV/Å, see Figure 17) was found to be 105 Mrad(Si).

To determine the total dose, one must first calculate the fluence of the silicon ions in cm$^{-2}$,

$$\phi_{ion} = \frac{I \times t}{q \times A}, \tag{3.4}$$

where $I$ is the current of the beam in amperes, $t$ is the pulse duration in seconds, $q$ is the charge of an electron in coulombs, and $A$ is the area of the beam in $cm^2$. The beam current used was 600 pA with a pulse duration of 133 ms and a beam area of 1 $cm^2$, such that equation (3.4) yields a fluence of 5E8 $cm^{-2}$ per pulse; over two pulses, the total fluence became 1E9 $cm^{-2}$. The total dose in rad(Si) was calculated using the following equation:

$$Dose = \frac{Constant \times \left(\frac{dE}{dx}\right)_{elec} \times \phi}{\rho_{Si}}, \tag{3.5}$$

where the constant is $1.6 \times 10^{-6}$, $\left(\frac{dE}{dx}\right)_{elec}$ is the electrical (ionization) energy loss calculated by the Stopping and Range of Ions in Matter (SRIM) simulation program (eV/Å), $\phi$ is the fluence of the ion beam ($cm^{-2}$), and  is the density of silicon (2.32 $g/cm^3$). The constant is necessary to convert the values in their specified units to 0.01 J/kg, which are the units for 1 rad.

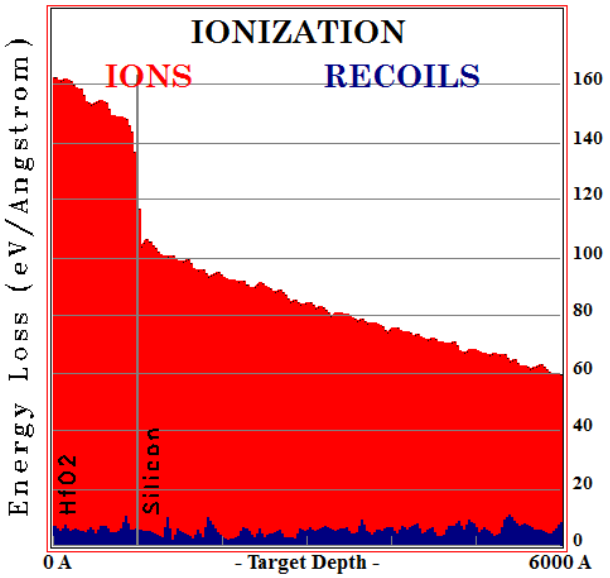


**Figure 17. TRIM simulation for 1 MeV $^{+}1$ silicon ions hitting PLD $HfO_2$. Average value in $HfO_2$ is approximately 152 eV/Å, which is the number used to calculate the total dose in rad(Si).**

As shown in Table 3, the ALD samples experienced ionizing radiation of varying fluence levels (1E8 $cm^{-2}$, 1E9 $cm^{-2}$, and 5E10 $cm^{-2}$). Irradiation was done at Sandia National Laboratories using $^{+}1$ nitrogen ions with 20 keV energy. Using equation (3.5), the total dose was determined to be 448 Mrad(Si) at a fluence of 5E10 $cm^{-2}$, 9 Mrad(Si) at a fluence of 1E9 $cm^{-2}$, and 0.9 Mrad(Si) at a fluence of 1E8 $cm^{-2}$; the average ionizing energy loss was found to be approximately 13 eV/Å using SRIM.

# IV. Results and Analysis

## Chapter Overview

This chapter will discuss and attempt to explain the results obtained. More specifically, a discussion of penetration depth predicted by Monte Carlo simulations, Rutherford backscattering spectrometry results, quality of samples produced by different growth methods and/or conditions, radiation effects, and the spectra's dependence on energy (i.e. penetration depth). The spectral calibration of the equipment used will also be discussed. As an overview, a table of features found is presented and will be explained in further detail presently.

**Table 4. Overview of features found in $HfO_2$, given in both wavelength and energy, along with each feature's suspected source.**

| Wavelength (Å) | Energy (eV) | Suspected Source |
|---|---|---|
| 2100 | 5.905 | band gap |
| 3100 | 4.000 | oxygen vacancy |
| 4100 | 3.024 | grating |
| 4700 | 2.638 | grating |
| 6700 | 1.851 | grating |

It should be noted that $SiO_2$ is known to form at the interface between $HfO_2$ and Si; peaks have been found to occur at 2800, 4450, 4800, 5200, and 6400 Å [28]. Table 4 does not contain any of these peaks because the boundary was not examined in this experiment, as will be shown with the following description of the Monte Carlo simulation.

**Monte Carlo Simulation**

To determine the penetration depth of the incident electrons and thus the depth at which the luminescence is originating, a Monte Carlo simulation was performed for $HfO_2$ on Si at a thickness of 50 nm and a density of 9.68 g/cm. For an electron beam energy of 5 keV, it was found that the majority of the electrons deposit their energy within the first 25 nm of $HfO_2$. Electrons that reach the silicon will only serve to decrease the intensity of the signal because silicon's band gap is too small (too long a wavelength, ~11,000 Å) to be seen; both the grating and photocathode used are only able to detect wavelengths up to 8000 Å. As a future study, it would be useful to examine the $HfO_2$/Si interface to see if any $SiO_2$ has formed; because the 4100Å and 4700 Å peaks have yet to be explained, a more complete depth-resolved study through the interface may prove that these peaks are related to $SiO_2$ forming at the boundary layer. This would present itself as an increase in these intensities with respect to the primary peak at 3100 Å. It is more likely, though, that the peaks at 4100Å and 4700 Å are due to some contaminant in the chamber; we suspect a contaminant because these same peaks are also seen in two other materials that were examined in the same chamber, namely lithium tetraborate and aluminum gallium nitride. Spectra are presented in Figure 19 that appear to have matching peaks across assorted materials, with clear peaks at 4100Å, 4700 Å and 6700 Å, to name a few.

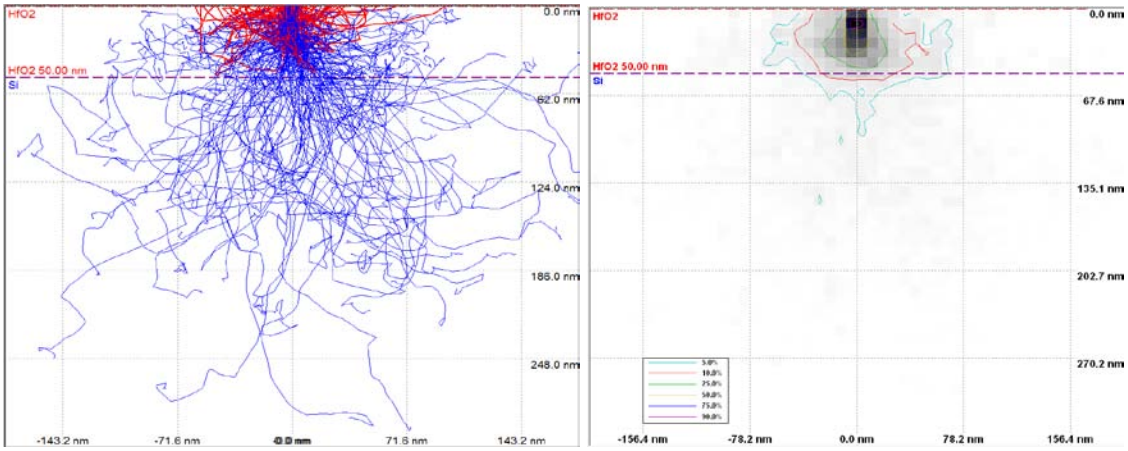


(a) (b)

**Figure 18. (a) Monte Carlo simulation of 50 nm $HfO_2$ at 5 keV, primary (blue) and backscattered (red) electron trajectories. (b) Monte Carlo simulation under same parameters, showing assorted percentages of electrons reaching the depth and span shown. Note that the bulk of the electrons stay within the $HfO_2$, with only 10% of the electrons having enough energy to cross into the silicon substrate.**

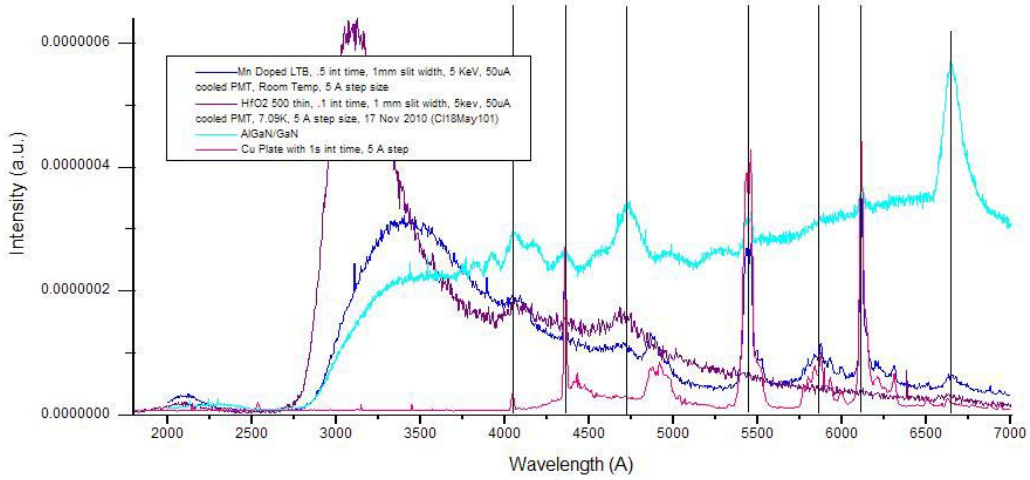


**Figure 19. Compilation graph of manganese doped lithium tetraborate, PLD $HfO_2$ deposited on 500°C silicon substrate, AlGaN on GaN, and the copper plate on which all samples were mounted. This shows the clear presence of contamination in the chamber whose peaks appear at the plotted vertical lines that encompass each separate material.**

## Rutherford Backscattering Spectrometry

RBS was performed by Captain Foster at the Ion Beam Laboratory (IBL) at SNL using 2 MeV helium ions in the +2 charge state; this was done in order to determine thickness and stoichiometry. Measurements were taken on four samples: 500°C thin,

750°C thin, and two ALD samples from the same batch that claimed to be at a thickness of 50 nm. All samples were measured as-grown.

The varying peak widths in Figure 20 illustrate the difference in thicknesses of the two thin samples; the 500°C thin sample was found to have a thickness of 82.45 nm while the 750°C thin sample was found to have a thickness of 148.1 nm. The deposition of $HfO_2$ was therefore inconsistent between batches. To determine if PLD is also non-uniform across the same batch, more RBS measurements would need to be taken. RBS found the thickness of ALD samples to be very consistent and accurate. The stoichiometry is also consistent, but gives an oxygen-rich material.

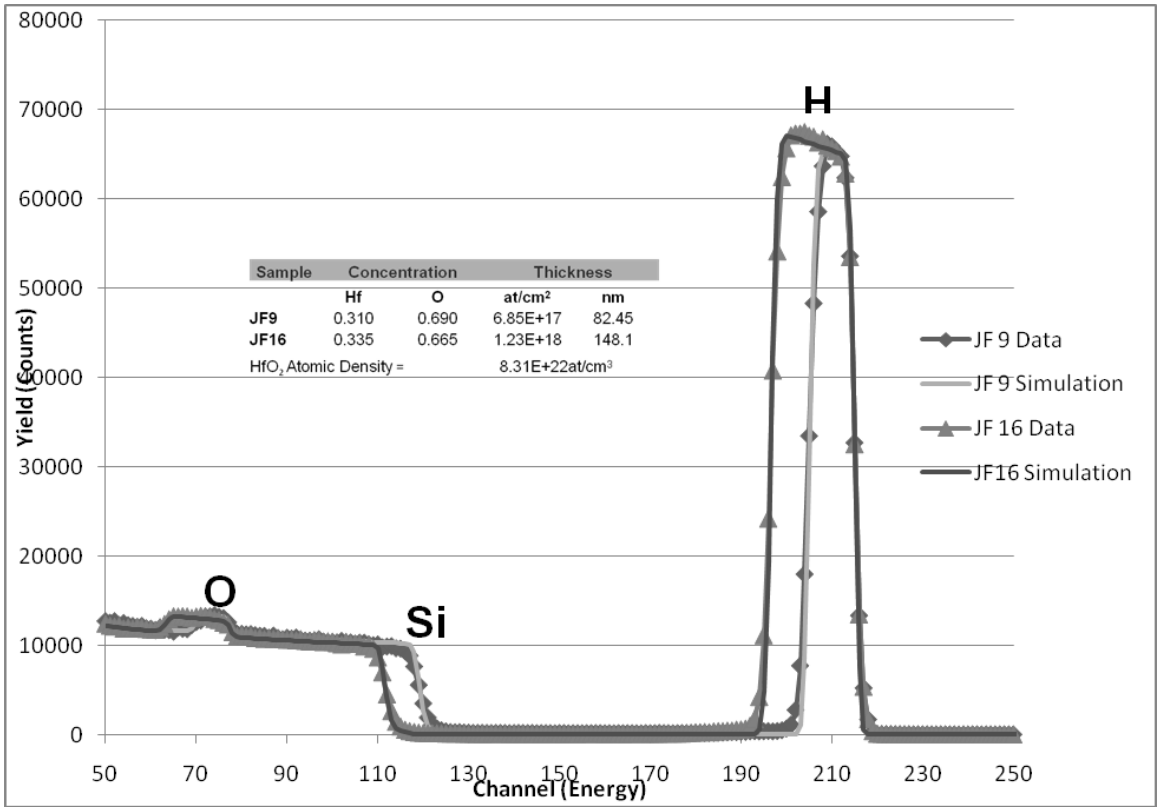


**Figure 20. Rutherford backscattering spectrometry of 500°C thin (JF9) and 750°C thin (JF16). Thicknesses were found to vary significantly between thin batches. Stoichiometry for 500°C thin was found to be oxygen-rich.**

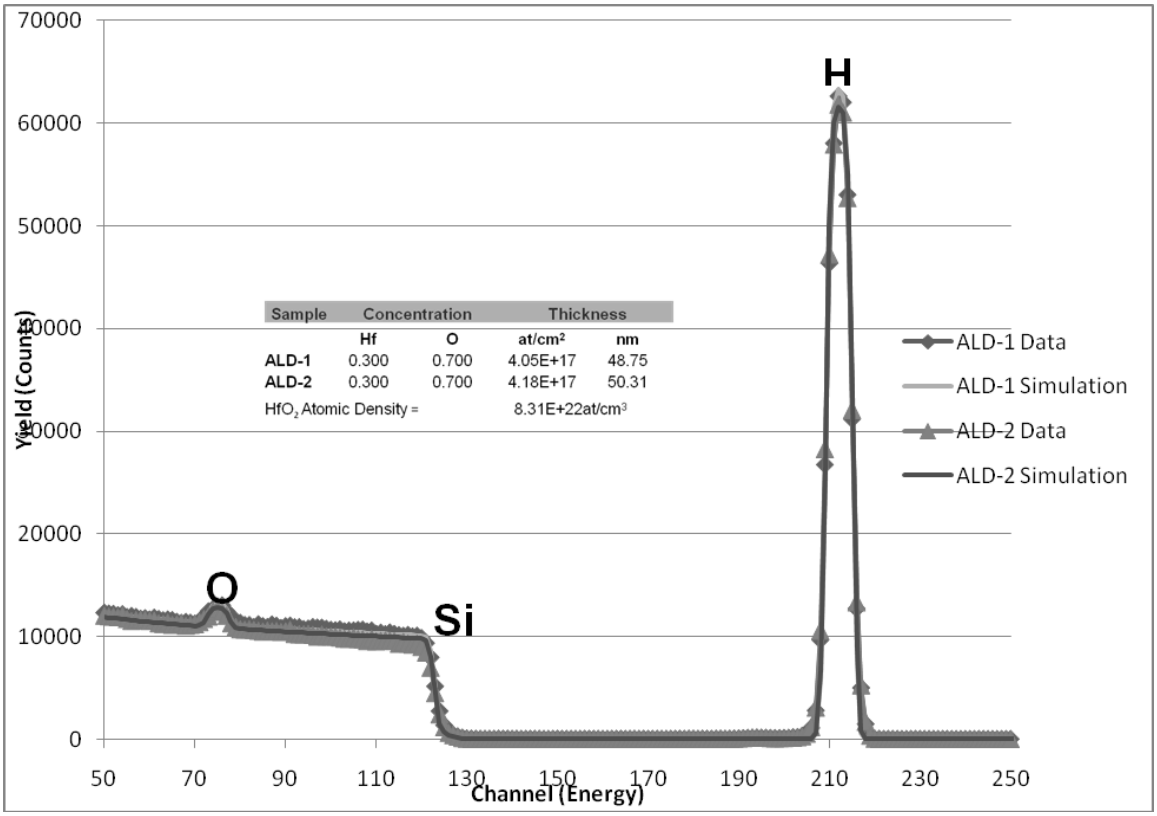


**Figure 21. Rutherford backscattering spectrometry of two ALD samples from the 50 nm batch. Thicknesses were found to be consistent. Stoichiometry for ALD samples was found to be oxygen-rich.**

## Growth Methods and Conditions

Cathodoluminescence measurements were taken for each substrate deposition temperature. Results show that the features in each sample were consistent with respect to their wavelengths, but the intensities relative to the other features changed from sample to sample. As previously discussed, the substrate temperature affects surface diffusion, which would imply a higher density for the material at a higher substrate temperature during growth. One can see that the feature at 3100 Å grows in relation to the features at 4100 Å and 4700 Å as the substrate temperature increases. This growth is consistent with the literature in that 3100 Å (~4 eV) has been associated with the $HfO_2$ itself (more

specifically, to oxygen vacancies within the material); as the density increases, so should the intensity of features seen.

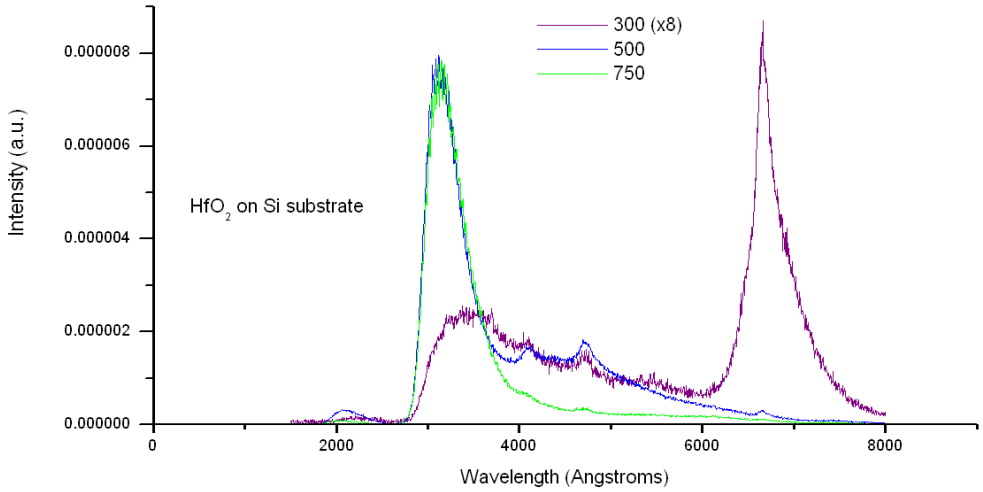


**Figure 22. Pulsed laser deposited $HfO_2$ on Si substrate. 300°C substrate deposition temperature (purple), 500°C substrate deposition temperature (blue), and 750°C substrate deposition temperature (green). Data were taken at a chamber temperature of 8K, a beam energy of 5 keV, and a beam current of 30 µA. This figure shows that features appear at the same wavelengths but with different relative intensities.**

A further analysis of the 300°C and 500°C samples was performed by Dr. Peter Dowben of the University of Nebraska – Lincoln using X-ray diffraction (XRD), in which the atomic structure is found based on the elastic scattering of X-rays from the electron clouds of the individual atoms. A comparison of Figure 23 and Figure 24 shows that the features present in both the 300°C and 500°C samples are consistent, but the spectrum for the latter shows the features to be better defined (less broadened) and the signal-to-noise ratio to be higher. The double peak present in Figure 24 at approximately 35° is only seen as a single peak in Figure 23 because the latter has been broadened too much. This implies that samples grown at 500°C are of better quality than those grown at 300°C. We hypothesize that this directly correlates to the density of the samples that was discussed previously, with the density being higher and more consistent when grown at

higher temperatures. We are not currently in possession of XRD data for the 750°C samples or the ALD samples, but we conjecture that the 750°C sample will be of better quality than the 500°C sample. This relationship of quality to density would also imply that the feature seen at 3100 Å also represents the quality of the material, with an increase in its intensity relative to the 4100 Å and 4700 Å features presenting a better (more consistent density) material.

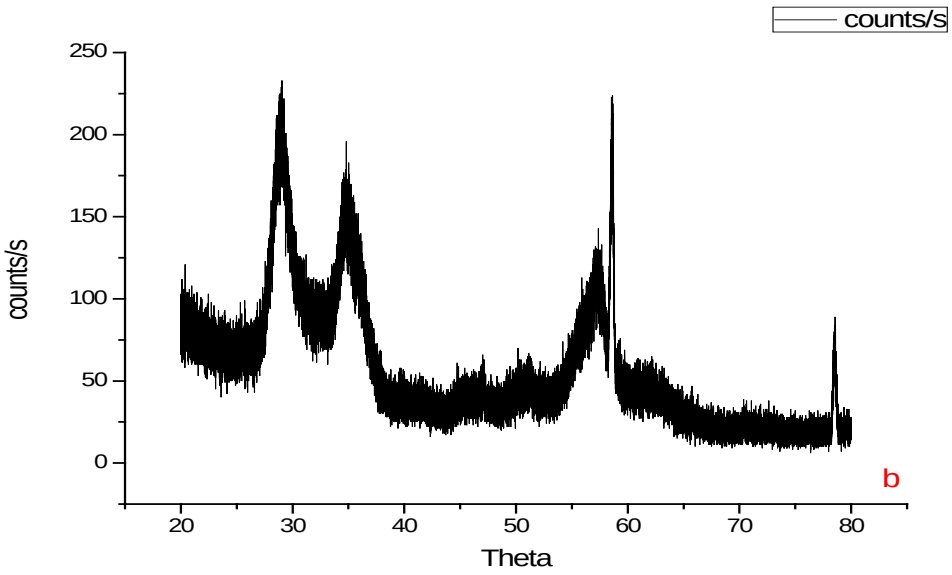


**Figure 23. XRD of 300°C thick sample.**

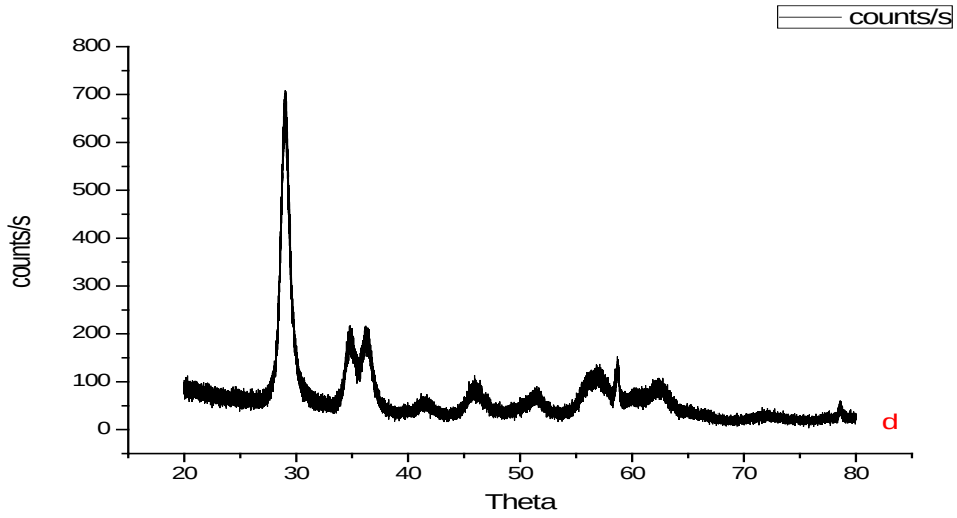


**Figure 24. XRD of 500°C thick sample.**

If the relative height of the 3100 Å feature truly does represent the quality of the material, Figure 25 would suggest that the ALD sample, grown at a substrate temperature of 250°C, is of better quality than the 300°C PLD sample, even though the growth temperature was lower, but not better than the 500 °C or 750°C PLD samples. One must now consider the quality of the two growth methods under similar conditions. Without XRD data, one might suppose that ALD produces better quality materials when grown at equivalent substrate temperatures if only because the ALD samples appear to have a more consistent thickness throughout the material as their surface appearance is very uniform and of only one color compared to drastic color gradients across only a few millimeters of the PLD samples, probably due to varying film thicknesses. One could then suppose that the ability to produce a consistent thickness is related to the ability to produce a consistent density, which would then account for the 3100 Å feature being more prevalent in the ALD sample than the 300°C PLD sample.

Based on the XRD spectra presented in Figure 23 and Figure 24 and comparing with the known monoclinic phase presented in Figure 9, it appears that neither the 300°C nor 500°C PLD thin samples are monoclinic. The (111) plane is not present in our data, nor is the (320) plane or the (100) plane. Our samples are clearly not amorphous, but without known XRD spectra on the tetragonal and orthorhombic phases, we cannot determine the structure of our $HfO_2$ samples. The fact that the aforementioned planes are not present in our spectra may not rule out the structure being monoclinic, though, unless the tetragonal and orthorhombic phases show no similarities to the monoclinic phase. Because temperature appears to be the main factor in determining crystal structure as discussed in Chapter II, one can suppose that the ALD samples will be of similar structure to the 300°C PLD samples.

There is another aspect of the ALD samples to consider, though. Rutherford backscattering spectrometry was performed on both PLD and ALD samples. Stoichiometry for the PLD samples was found to be 33% Hf and 66% O, as expected. Stoichiometry for the ALD samples was found to be 30% Hf and 70% O, which is oxygen-rich. If the peak at 3100 Å is truly related to oxygen vacancies in the material, an oxygen-rich material would show that feature to have greatly decreased in intensity relative to the rest of the spectrum. This could mean one of two things: either that samples grown by ALD with proper stoichiometry would lead to a more prominent feature at 3100 Å (i.e. a better material) with the growth conditions being slightly wrong, or that the method of ALD is inherently worse than PLD because stoichiometry is harder to control.

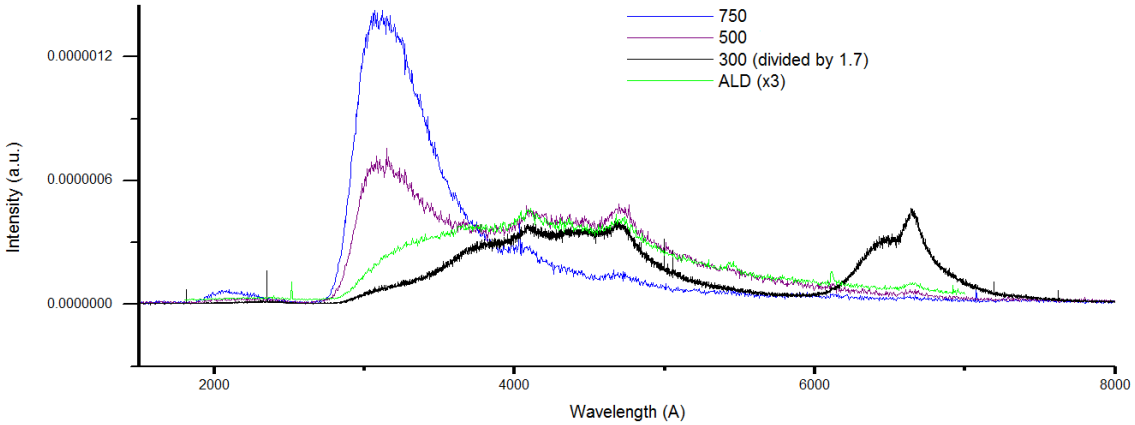


**Figure 25. ALD compared to PLD samples. All spectra were obtained at room temperature prior to any irradiation. Intensities have been scaled for a better comparison.**

## Radiation Effects

Data collected show that there appear to be minimal changes after irradiation, at least at the dose levels to which the samples were exposed. Intensities do appear to change, but one must remember that the intensity is all relative, and can change drastically for the same sample if the optics were not realigned precisely as before, or if the beam shape or position were to change.

Ignoring the peak at 6700 Å, Figure 26 shows that features agree between unirradiated 300°C samples and gamma irradiated 300°C samples. There is a noticeable shape change, though, at 3100 Å. For the samples that have been cooled by the liquid helium refrigerator to ~7 K, it becomes apparent that this feature has increased in intensity relative to the other features and is much less prominent at room temperature. This can be accounted for by the known reduction in lattice vibrations at colder temperatures. This feature has been associated with the bulk of $HfO_2$, indicating that fewer phonons will allow more energy to be emitted in the form of radiative transitions (i.e., photons), thus increasing the intensity of that feature.

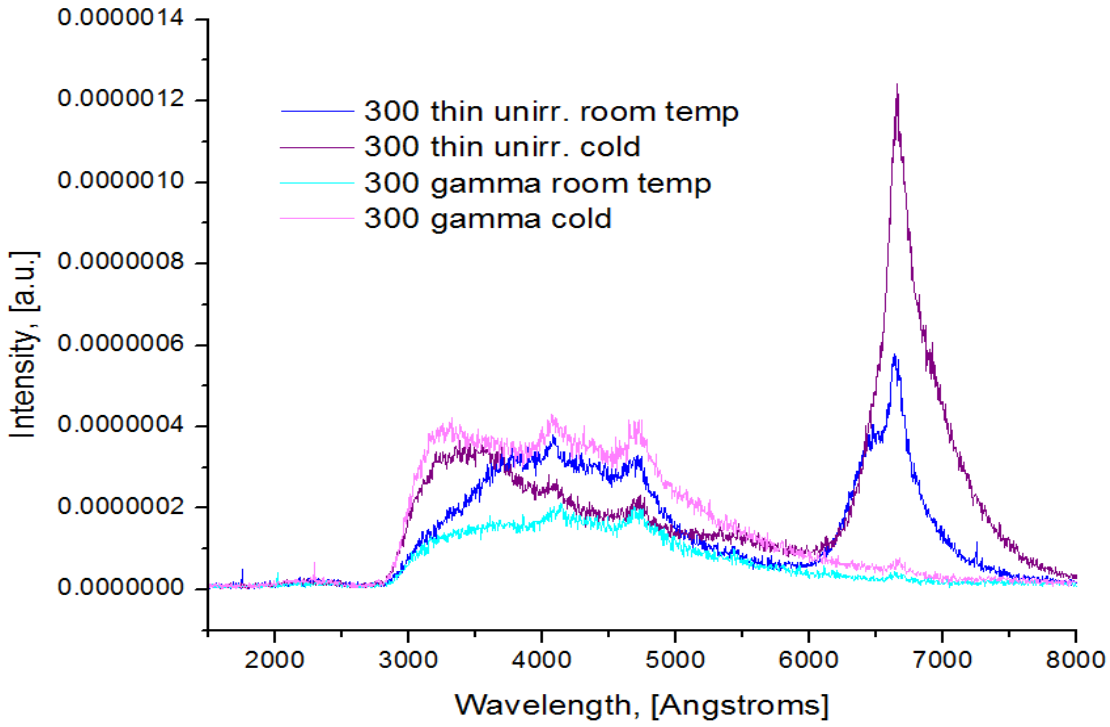


**Figure 26. 300°C PLD samples, both unirradiated and gamma irradiated. Measurements were taken at 7 K and at room temperature.**

As presented in Table 2, the only batch of samples from which we have all three types of irradiation is the 750°C thin PLD batch, which is why it was chosen to represent the changes after irradiation, presented in Figure 27; additionally, it is suspected to be of the best quality among all sample batches. Unirradiated ALD is also presented in the figure for a more detailed shape comparison and emphasis on the feature alignment across growth methods.

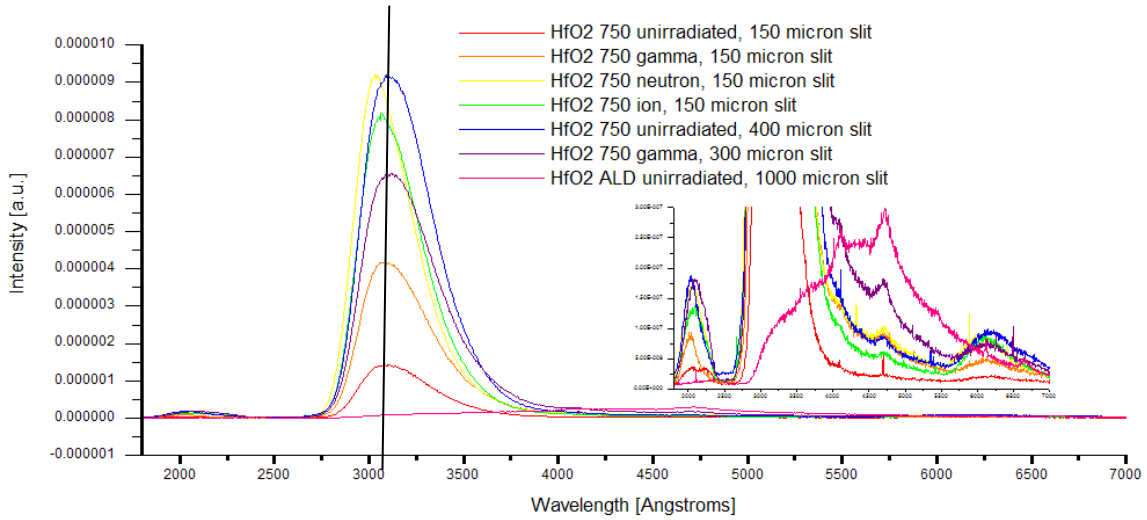


**Figure 27. Compilation graph of PLD $HfO_2$ with a silicon substrate temperature of 750°C during deposition; ALD unirradiated sample is also shown to emphasize the difference in shape as a result of the growth method used. All spectra were obtained at a sample temperature of 7 K.**

From the figure, it is apparent that the feature at 3100 Å does not actually remain at that wavelength; it shifts to a lower wavelength after both neutron and ion irradiation, and to a higher wavelength after gamma irradiation. A possible explanation for this shift is that the feature at 3100 Å is not actually one single peak, but two peaks; this would also account for the shape of the feature being stretched to the right and not following a normal Gaussian distribution. If this feature consists of two peaks, then it seems that the ion and neutron irradiation are affecting one of the peaks while the gamma irradiation is affecting the other. Generally, the irradiation would cause a decrease in intensity and not an increase, so one could assume that the ion and neutron radiation are affecting the right peak, letting the left peak be more dominant and thus pull the feature to a lower wavelength; likewise, the gamma radiation is assumed to be affecting the left peak. The problem with associating this feature with two peaks, though, is that this no longer agrees with published literature on the matter of oxygen vacancies accounting for one single

transition at that wavelength. Currently, this presents an irresolvable dilemma that should be investigated further. Regardless, this could suggest that there is some level of damage occurring in the sample.

Ion irradiation of ALD samples also showed minimal effects. Figure 28 shows a comparison between unirradiated and ion irradiation at three different fluence levels. Among the ion irradiated samples, one can see that the three fluence levels produce identical results. Continuing with the supposition that irradiation caused damage at the 3100 Å feature (regardless of whether it is comprised of two peaks or one), Figure 28 shows a decrease in intensity at that wavelength, seen as a more curved transition from 3000 Å to 4000 Å, approximately, in the unirradiated sample than in the irradiated samples, which show a very steep, straight transition. It is suspected that some damage is occurring in the form of a decrease in CL intensity of the 3100 Å peak.

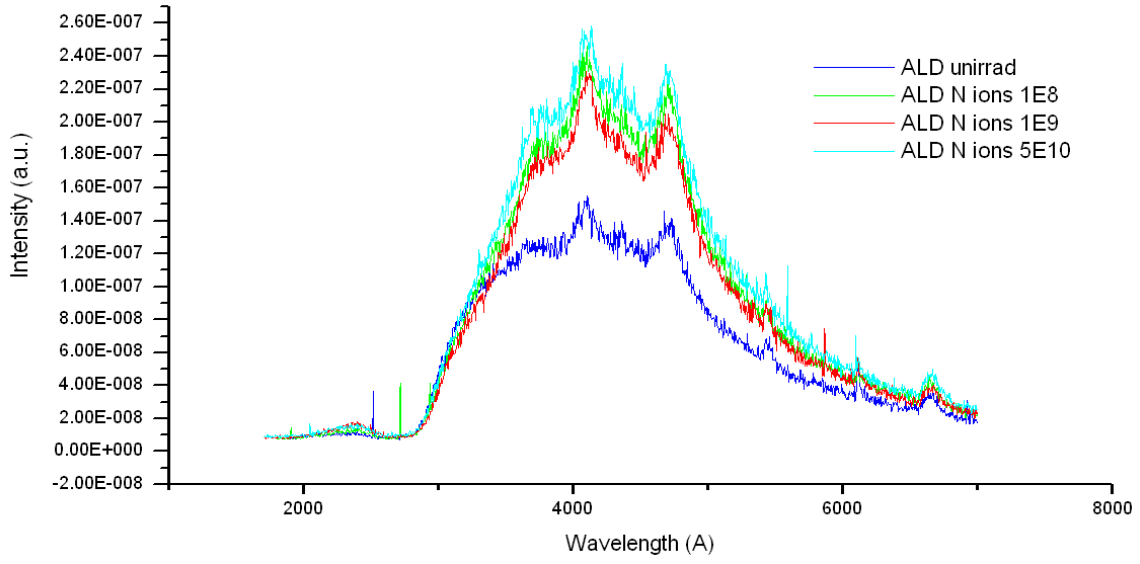


**Figure 28. ALD samples, 50 nm thick. Samples include unirradiated, $1x10^{8}$ $cm^{-2}$ fluence, $1x10^{9}$ $cm^{-2}$ fluence, and $5x10^{10}$ $cm^{-2}$ fluence. Measurements were taken at room temperature.**

**Energy Dependence**

As previously discussed, varying the energy of the electron beam allows one to probe different depths of a material. With the thickness of the 500°C samples already determined to be approximately 80 nm, CASINO shows that an energy of 7.5 keV will keep the majority of the energy within the $HfO_2$. Figure 29 shows a range of beam energies from 1.5 keV to 7.5 keV probing a 500°C gamma irradiated sample at room temperature. It is evident that the features present remain consistent throughout the different depths, showing that the sample is consistent through the thickness examined.

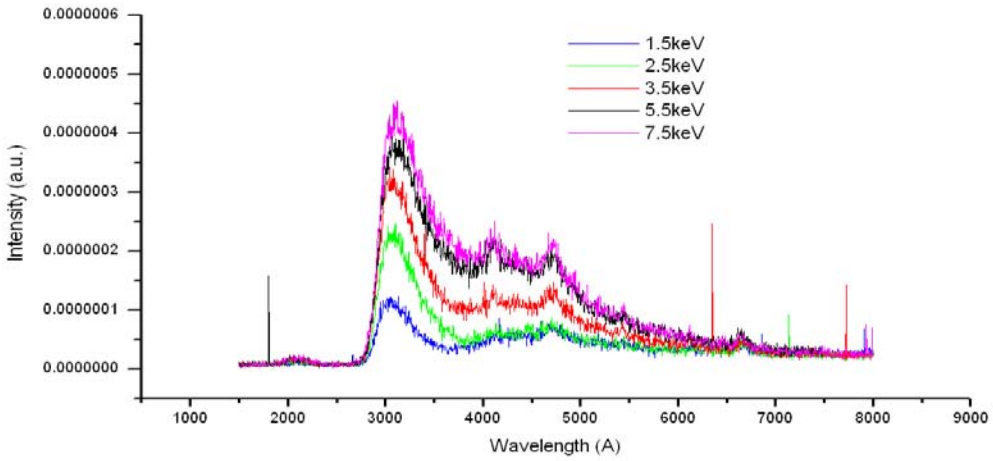


**Figure 29. 500°C PLD sample, gamma irradiated. Measurements were taken over a range of energies at room temperature.**

Figure 30 presents a similar conclusion as the previous figure, with unirradiated ALD being examined at room temperature. Beam energy ranged from 1 keV to 10 keV, which still found the spectra to maintain a constant shape throughout the entire depth examined. Similar results were obtained for other samples examined, but all spectra need not be shown.

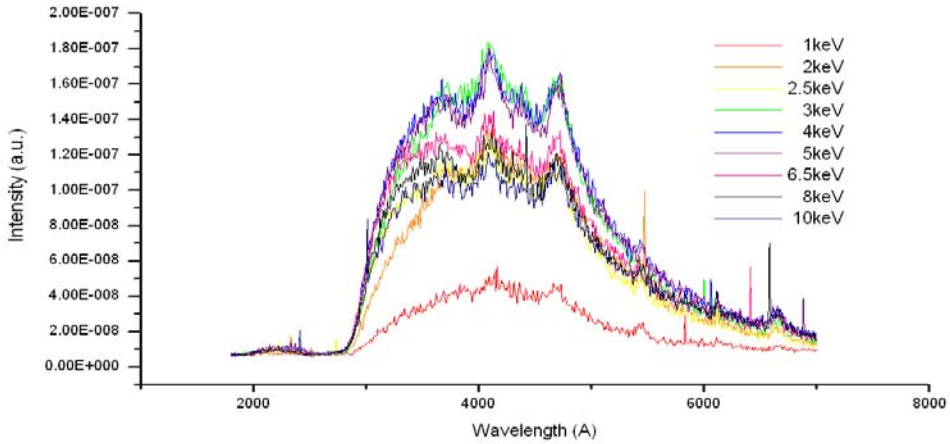


**Figure 30. ALD sample, 50 nm thick and unirradiated. Plot shows energy dependence of the sample at room temperature.**

## Spectral Response of the Experimental System

Near the completion of this research project, it was observed that certain peaks in the data appeared not only in the $HfO_2$, but also in spectra from a research project on lithium tetraborate and even from the sample holder itself, which should have no spectrum at all. To resolve this issue, the spectral response of the system was measured. Initially a system response spectrum using a calibrated blackbody source set to 1350°C was run. Using Planck's Radiation Law,

$$I_\lambda = \frac{2\pi hc^2}{\lambda^5}\left[\frac{1}{e^{\frac{hc}{\lambda k_B T}} - 1}\right], \tag{4.1}$$

where $I_\lambda$ is the spectral irradiance in $J/m^3/s$, $h$ is Planck's constant in $J$-$s$, $c$ is the speed of light in $m/s$, $k_B$ is Boltzmann's constant $J/K$, $T$ is temperature in $K$, and $\lambda$ is the wavelength in $m$ [29]. Figure 31 (b) shows the region of interest of the Planckian distribution, and Figure 32 shows the actual response of the system. One will notice that there is a definite peak at 6700 Å which should not be there but has consistently appeared

throughout our data. At this time, the source of this peak is not definitively identified but it is most probably an artifact of the grating.

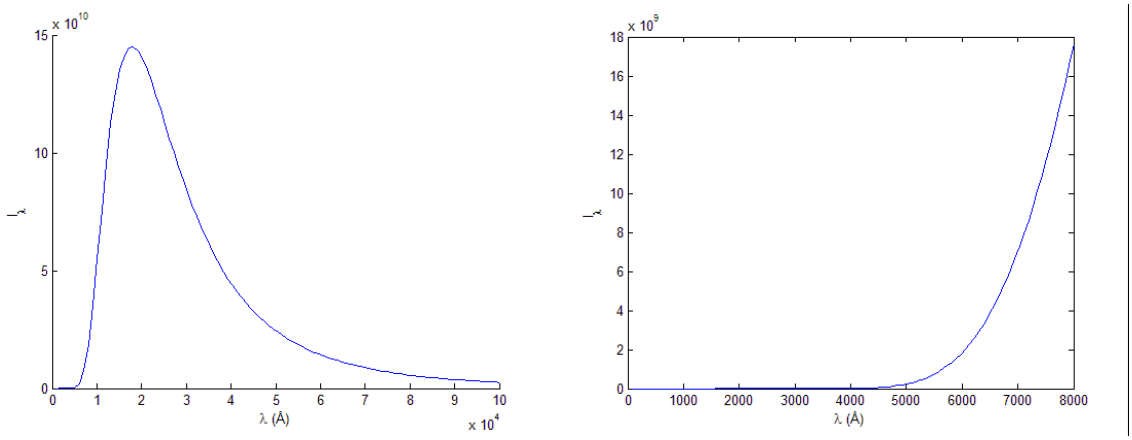


(a) (b)

**Figure 31. Planck's Radiation Law at T=1350°C. Plot (b) is a subset of plot (a), which shows the range of interest as limited by the capabilities of the photomultiplier tube.**

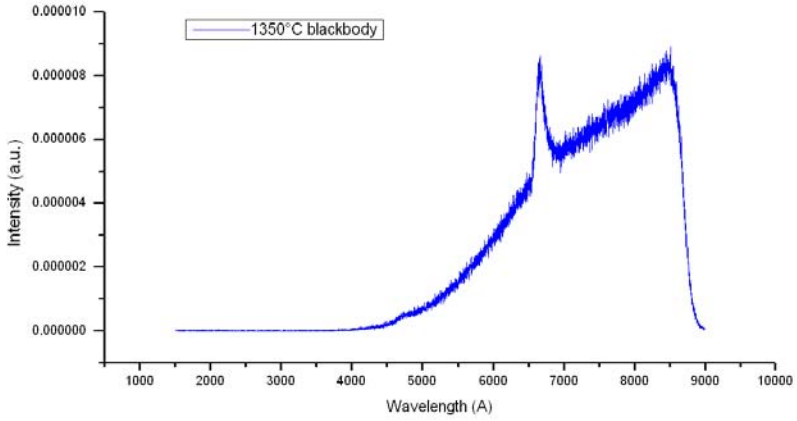


**Figure 32. Response curve of total Cathodoluminescence system (grating spectrometer and photomultiplier tube) using a blackbody source at 1350°C.**

A major problem with using a 1350°C blackbody for this response curve is that there is minimal intensity below 4000Å. Proper calibration would require a much hotter blackbody, which was not available. Since a calibrated blackbody source was unavailable, a white light source, similar to a quartz-iodine source, was placed in front of

the spectrometer. Figure 33 and 34 show spectra using this source obtained from the spectrometer and PMT used for the research presented in this thesis with that from a comparable spectrometer and PMT available in our lab. These spectra illustrate quite clearly that there are certain features inherent to the experimental measurement system that have been appearing in almost all the $HfO_2$ data taken but which are not associated with $HfO_2$ . Specifically, features at 4100, 4700, and 6700 Å appear in the first white light spectrum but not in the second spectrum. Furthermore, these peaks also appear in the CL spectrum taken from the brass sample holder. The holder, of course, being a metal and a conductor, should have no CL spectrum. Although time did not permit further study of these peaks as part of this thesis, they are undoubtedly associated with imperfections in or damage to the grating used.

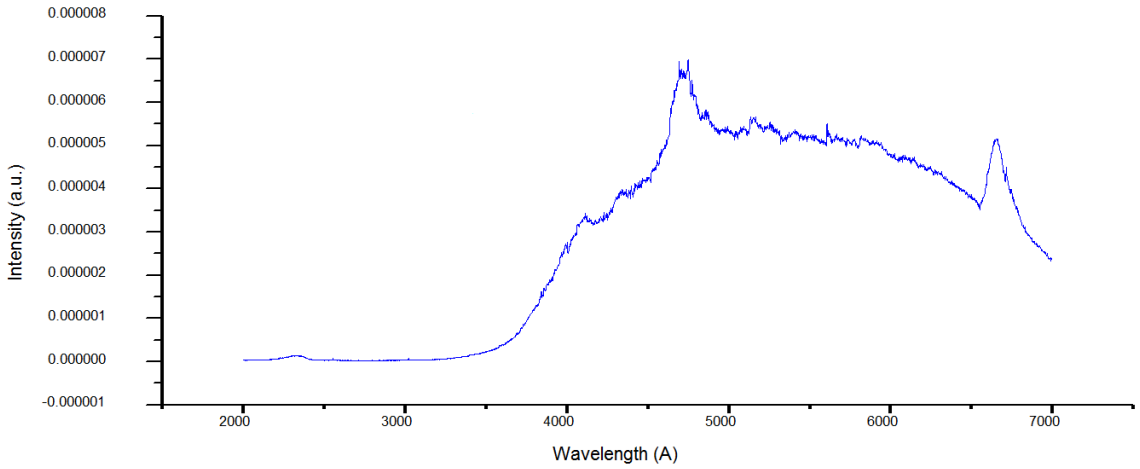


**Figure 33. Spectral response of white light source. Note the features appearing at 4100, 4700, and 6700 Å that have also appeared consistently throughout the $HfO_2$ spectra.**

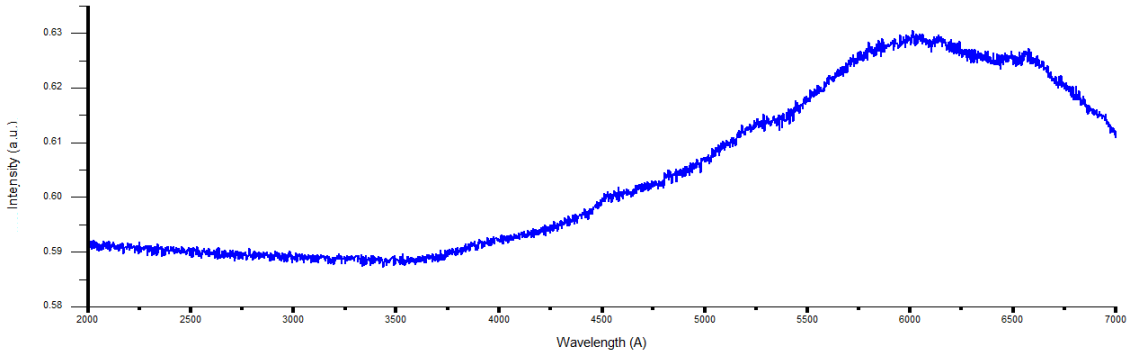


**Figure 34. Spectral response of the same white light source presented in Figure 33 measured on a second spectrometer and PMT. The spectrometer and PMT were the same models used previously, but the grating has a blaze wavelength of 5500 Å instead of 3300 Å, which is the cause of the overall shape change in the spectrum. Note that there are no longer any features at 4100, 4700, or 6700 Å, further emphasizing that those features are inherent to the detection system used.**

Thus all of the data taken in this thesis has been tainted with these three spurious peaks. As a result they have been ignored as best as possible in the analysis of the spectra. The conclusions reached are still valid, however, a more detailed and conclusive analysis might have been possible if the peaks were not present. They could have been removed graphically but since they exist to a lesser or greater extent in the various spectra depending on the intensity of the luminescence from the sample itself, it was decided that a better approach would be to rerun the significant data using the current results reported here as a guide. This must be left for a follow-on thesis or research project.

# V. Conclusions and Recommendations

## Conclusions of Research

Three conclusions can be arrived at from this study. The first is that $HfO_2$ appears to be relatively resistant to radiation when exposed to gamma irradiation using $^{60}Co$ at a dose of 1 Mrad (Si), neutron irradiation at a dose of 25 krad (Si), which is the 1 MeV neutron equivalent, ion irradiation using 1 MeV (+1) silicon ions at a dose of 70 krad (Si), and the same ion irradiation at a dose of 250 krad (Si). As a result, the radiation resistance of $HfO_2$ should continue to be studied but the dose levels should be increased. The second conclusion is that a higher substrate deposition temperature appears to produce a better PLD material. No such conclusion can be reached for the ALD material since only samples grown at one temperature were available. And third, significant improvement is required on the experimental system to guarantee untainted spectra.

## Significance of Research

For the radiation doses to which $HfO_2$ was exposed, it seems that $HfO_2$ is radiation hard; therefore, this material has yet to be disproved as a viable replacement for $SiO_2$ as the gate insulator in electronic devices used in radiation environments. Switching to $HfO_2$ from $SiO_2$ would allow for smaller devices to be fabricated without sacrificing capacitance or thickness. Furthermore, this research suggests that ALD may be preferred as a growth method for $HfO_2$ but a substrate temperature similar to that conducted for PLD material should be carried out. Additionally, this thesis contains information on the cathodoluminescence of $HfO_2$ itself, without doping or coatings, that has not been previously presented in any great detail. In addition, the discussion and analysis of

growth method quality was also lacking in research previously conducted by others. Finally, while bearing no significance to the scientific community as a whole, this research exposed unexpected problems with our experimental system, probably a defective grating, which needs to be rectified. Unfortunately, there was no clear indication of these problems until near the end of the study.

**Recommendations for Future Research**

It is recommended that the samples of $HfO_2$ be fully characterized, including thickness and crystal structure, as a means to better compare the samples in possession to samples studied in research previously conducted by others. Additionally, a study of the boundary layer between $HfO_2$ and Si might yield spectra more consistent with published data. A further study of the experimental system should also be conducted in order to eliminate any spurious peaks and guarantee quality spectra.

XRD data should be collected for all samples as a means of comparing and contrasting the quality of material produced by ALD versus PLD and of material grown at varying substrate temperatures. Irradiation should be performed at much higher doses to determine the extent to which $HfO_2$ is radiation hard. Gamma irradiation need not be performed, as damage is not expected to occur. Ion irradiation would be of greater interest because it is expected to cause displacement damage, which is likely to be seen by CL if the damage is prevalent enough.

## Bibliography


[1] X. Zhao and D. Vanderbilt. (2002, First-principles study of structural, vibrational, and lattice dielectric properties of hafnium oxide. *Physical Review B 65(23),* pp. 233106.

[2] M. C. Cheynet, S. Pokrant, F. D. Tichelaar and J. L. Rouvière. (2007, Crystal structure and band gap determination of HfO thin films. *J. Appl. Phys. 101*pp. 054101.

[3] J. Hecht, *Understanding Lasers.* Hoboken: John Wiley & Sons, 2001.

[4] B. D. Cullity, *Elements of X-Ray Diffraction.* Reading: Addison-Wesley, 1956.

[5] R. Eason, *Pulsed Laser Deposition of Thin Films.* Hoboken: John Wiley & Sons, 2007.

[6] D. L. Smith. (1995, *Thin-Film Deposition: Principles and Practice* .

[7] J. Petrosky. Radiation effects on electronic devices. *(January 5),* .

[8] Wikipedia, "Effective Atomic Number," vol. 2011, 2010.

[9] C. Claeys and E. Simoen, *Radiation Effects in Advanced Semiconductor Materials and Devices.* Berlin: Springer-Verlag, 2002.

[10] S. O. Kucheyev, M. Toth, M. R. Phillips, J. S. Williams, C. Jagadish and G. Li. (2001, Cathodoluminescence depth profiling of ion-implanted GaN. *Appl. Phys. Lett. 78*pp. 34.

[11] M. Fox, *Optical Properties of Solids.* New York: Oxford University Press, 2010.

[12] B. G. Yacobi and D. B. Holt, *Cathodoluminescence Microscopy of Inorganic Solids.* New York: Plenum Press, 1990.

[13] D. Drouin, A. R. Couture, D. Joly, X. Tastet, V. Aimez and R. Gauvin, "Casino V2.42--A Fast and Easy-to-use Modeling Tool for Scanning Electron Microscopy and Microanalysis Users," *Scanning,* vol. 29, pp. 92, 2007.

[14] P. Hovington, D. Drouin and R. Gauvin. (1997, CASINO: A new monte carlo code in C language for electron beam interaction-part I: Description of the program. *Scanning 19(1),* pp. 1-14.

[15] D. C. Joy and S. Luo. (1989, An empirical stopping power relationship for low-energy electrons. *Scanning 11(4),* pp. 176–180.

[16] Z. Czyżewski, D. O. N. MacCallum, A. Romig and D. C. Joy. (1990, Calculations of mott scattering cross section. *J. Appl. Phys. 68*pp. 3066.

[17] T. Ito, M. Maeda, K. Nakamura, H. Kato and Y. Ohki. (2005, Similarities in photoluminescence in hafnia and zirconia induced by ultraviolet photons. *J. Appl. Phys. 97*pp. 054104.

[18] Y. M. Strzhemechny, M. Bataiev, S. P. Tumakha, S. H. Goss, C. L. Hinkle, C. C. Fulton, G. Lucovsky and L. J. Brillson. (2009, Low energy electron-excited nanoscale luminescence spectroscopy studies of intrinsic defects in $HfO_2$ and $SiO_2$-$HfO_2$-$SiO_2$-si stacks. *Journal of Vacuum Science & Technology B: Microelectronics and Nanometer Structures 26(1)*, pp. 232-243.

[19] J. G. Mendoza, M. A. Aguilar Frutis, G. A. Flores, M. G. Hipólito, A. Maciel Cerda, J. A. Nieto, T. R. Montalvo and C. Falcony. (2010, Synthesis and characterization of hafnium oxide films for thermo and photoluminescence applications. *Applied Radiation and Isotopes 68(4-5)*, pp. 696-699.

[20] T. P. Smirnova, V. V. Kaichev, L. V. Yakovkina, V. I. Kosyakov, S. A. Beloshapkin, F. A. Kuznetsov, M. S. Lebedev and V. A. Gritsenko. (2008, Composition and structure of hafnia films on silicon. *Inorganic Materials 44(9)*, pp. 965-970.

[21] J. Wang, Y. Xia, Y. Shi, Z. Shi, L. Pu, R. Zhang, Y. Zheng, Z. Tao and F. Lu. (2007, 1.54 μm photoluminescence emission and oxygen vacancy as sensitizer in er-doped HfO films. *Appl. Phys. Lett. 91*pp. 191115.

[22] J. Aarik, H. Mändar, M. Kirm and L. Pung. (2004, Optical characterization of HfO2 thin films grown by atomic layer deposition. *Thin Solid Films 466(1-2)*, pp. 41-47.

[23] A. A. Rastorguev, V. I. Belyi, T. P. Smirnova, L. V. Yakovkina, M. V. Zamoryanskaya, V. A. Gritsenko and H. Wong. (2007, Luminescence of intrinsic and extrinsic defects in hafnium oxide films. *Phys. Rev. B 76(23)*, pp. 235315-1-235315-6.

[24] S. Walsh, L. Fang, J. K. Schaeffer, E. Weisbrod and L. J. Brillson. (2007, Process-dependent defects in Si/$HfO_2$/Mo gate oxide heterostructures. *Appl. Phys. Lett. 90(5)*, pp. 052901.

[25] A. A. Rastorguev, V. I. Belyi, T. P. Smirnova and L. V. Yakovkina, "Photoluminescence study of the electronic structure of $HfO_2$ films," *J. Struct. Chem.*, vol. 49, pp. 21-30, 2008.

[26] J. L. McFall, "Optical Investigation of Molecular Beam Epitaxy $Al_xGa_{1-x}N$ to Determine Material Quality," 2000.

[27] Wikipedia, "Einzel Lens," vol. 2011, 2010.

[28] M. Yoshikawa, K. Matsuda, Y. Yamaguchi, T. Matsunobe, Y. Nagasawa, H. Fujino and T. Yamane. (2002, Characterization of silicon dioxide film by high spatial resolution cathodoluminescence spectroscopy. *J. Appl. Phys. 92*pp. 7153.

[29] E. Hecht, *Optics.* San Francisco: Addison Wesley, 2002.

# REPORT DOCUMENTATION PAGE

*Form Approved*
*OMB No. 074-0188*



| 1. REPORT DATE *(DD-MM-YYYY)* | 2. REPORT TYPE | 3. DATES COVERED *(From – To)* |
|---|---|---|
| 24-03-2011 | Master's Thesis | June 2010 – March 2011 |

**TITLE AND SUBTITLE**

Cathodoluminescence of Irradiated Hafnium Dioxide

**5a. CONTRACT NUMBER**

**5b. GRANT NUMBER**

**5c. PROGRAM ELEMENT NUMBER**

**6. AUTHOR(S)**

Purcell, Emily A., Second Lieutenant, USAF

**5d. PROJECT NUMBER**

**5e. TASK NUMBER**

**5f. WORK UNIT NUMBER**

**7. PERFORMING ORGANIZATION NAMES(S) AND ADDRESS(S)**
Air Force Institute of Technology
Graduate School of Engineering and Management (AFIT/ENP)
2950 Hobson Way, Building 640
WPAFB OH 45433-8865

**8. PERFORMING ORGANIZATION REPORT NUMBER**

AFIT/GAP/ENP/11-M08

**9. SPONSORING/MONITORING AGENCY NAME(S) AND ADDRESS(ES)**
Defense Threat Reduction Agency
COL Mark Mattox
1900 Wyoming Blvd SE
Kirtland AFB, NM 87117-5669

**10. SPONSOR/MONITOR'S ACRONYM(S)**

DTRA/OP-CSU

**11. SPONSOR/MONITOR'S REPORT NUMBER(S)**

**12. DISTRIBUTION/AVAILABILITY STATEMENT**
APPROVED FOR PUBLIC RELEASE; DISTRIBUTION UNLIMITED.

**13. SUPPLEMENTARY NOTES**

**14. ABSTRACT**
The purpose of this research is to understand the effect of radiation on $HfO_2$ thin films, and to compare the quality of $HfO_2$ thin films produced by both atomic layer deposition (ALD) and pulsed laser deposition (PLD); PLD samples had varying substrate temperatures during deposition (300°C, 500°C, and 750°C). The entirety of this research was conducted using cathodoluminescence (CL) as the examination method. The excitation source was a Kimball Physics EMG-12 electron gun. The photomultiplier tube contained a gallium arsenide photocathode. Measurements were made with beam energies ranging from 1 to 10 keV and beam currents ranging from 30 to 50 μA, both at room temperature and at 7K. The experimentally-determined band gap of $HfO_2$ was consistent with published data, but many other features found in the literature were not present in the CL data obtained. $HfO_2$ appeared to be radiation hard up to the levels of radiation to which it was exposed. A higher substrate temperature during deposition for PLD samples produced a better material than lower temperatures. ALD produced a more consistent thickness but PLD ultimately produced a better quality material with respect to the spectrum obtained.

**15. SUBJECT TERMS**
Cathodoluminescence, hafnium dioxide, PLD, ALD, high-k dielectric

| 16. SECURITY CLASSIFICATION OF: | | | 17. LIMITATION OF ABSTRACT | 18. NUMBER OF PAGES | 19a. NAME OF RESPONSIBLE PERSON |
|---|---|---|---|---|---|
| a. REPORT | b. ABSTRACT | c. THIS PAGE | | | Robert L. Hengehold, PhD AFIT/ENP |
| U | U | U | UU | 82 | 19b. TELEPHONE NUMBER *(Include area code)* (937) 255-3636, ext 4502 (Robert.Hengehold@afit.edu) |

**Standard Form 298 (Rev. 8-98)**
Prescribed by ANSI Std. Z39-18